

A time-adaptive optimization approach for reconstructing immune response in a mathematical model of acute HIV infection using clinical data

L. Beilina *

I. Gainova †

G. Bocharov ‡

Abstract

The paper proposes a time-adaptive optimization approach for determining the time-dependent immune response function in a mathematical model of acute HIV infection, using clinical data from four untreated patients. We formulate the problem as a parameter identification problem for an immune response system of ODE which includes novel component integrated into the third equation of the classical three-equation HIV model. Tikhonov's regularization method, Lagrangian approach, from which we derive the optimality conditions, and a numerical scheme to solve the forward and adjoint problems, as well as parameter identification problem, are presented.

Three different a posteriori error estimates are derived and based on these estimates a time adaptive optimization algorithm is formulated. Numerical experiments demonstrate the effectiveness of the proposed adaptive method in reconstructing the immune response function during the acute phase of HIV infection, using patient-specific clinical data. Computational results show improvement of reconstruction of immune response function using the local time-adaptive mesh refinement method compared to the standard conjugate gradient method applied on a uniform time mesh.

1 Introduction

The mathematical modeling of immune dynamics is a foundational component of immunological research [15, 16, 20]. Although advanced experimental methods have significantly enhanced the analysis of immune function, mathematical modeling continues to play a crucial role in clinical applications—especially in tailoring individualized treatment strategies for pathological processes such that bacterial/viral infections or tumor growth. It is well established that physiological parameters differ across individuals. Consequently, developing robust and efficient parameter estimation methods is essential for integrating patient-specific data into mathematical models, thereby enabling truly personalized treatment strategies [11].

*Department of Mathematical Sciences, Chalmers University of Technology and University of Gothenburg, SE-42196 Gothenburg, Sweden, e-mail: larisa@chalmers.se

†Sobolev Institute of Mathematics SB RAS, 630090 Novosibirsk, Russia, e-mail: gajnova@math.nsc.ru

‡Marchuk Institute of Numerical Mathematics RAS, 119333 Moscow, Russia, e-mail: gbocharov@gmail.com

Parameter identification problem (PIP) for mathematical models frequently involves solution of nonlinear and ill-posed problems, making them particularly challenging to address through numerical methods [35, 36, 37]. The computational algorithms developed in this work are based on adaptive time-mesh refinement techniques for PIP for ODE or PDE – see recent advances in this area in [1, 14, 12, 13].

The primary objective of our work is to develop a time-adaptive algorithm for determining the immune response function within a mathematical model of untreated HIV infection. The model comprises a standard system of three ordinary differential equations (ODEs), enhanced by a novel component integrated into the third equation. In the recent work [1] the adaptive finite element method has been shown to significantly enhance parameter reconstruction when applied to assessing drug efficacy in the mathematical model of HIV infection proposed in [2].

In comparison to other optimal control algorithms used for solving parameter identification problems (PIPs), notable examples can be found in the works of [8, 10, 22] and references therein, our time-mesh refinement algorithm is based on rigorous finite element analysis for a posteriori error in the reconstructed parameter.

The approach proposed in this work is applicable to a wide range of parameter identification problems (PIPs), including more complex models of HIV infection that incorporate additional unknown functions and parameters –see, for example, HIV models proposed in [9, 25, 29, 31, 32, 33, 34, 39]. However, these models are substantially more complex than the three-equation system studied here and may be more appropriately addressed in future research.

The acute phase of HIV infection is associated with an exponential increase in viral load and, in most HIV infected individuals, begins with fever, headache, increased heart rate, and symptoms of viral spread to the lymphoid tissues (lymphadenopathy). The symptoms occur both before and at the peak of viremia and are relatively short in duration. The peak of viremia is more than 10^6 copies of RNA/ml of blood. After the peak, the viral load begins to decrease, both due to the body's immune response and due to the limited population of target cells (macrophages and CD4+ T-lymphocytes), and reaches a point of stabilization of the infectious process (so called as "viral equilibrium point"). The infection enters a chronic, latent phase, which can last several years.

Events occurring during the acute phase as well as quantitative characteristics, such as the level viral load at the point of stabilization of the infectious process and the level Target T cells at the end of the acute phase of HIV infection, are one of the factors determining the long-term development forecast diseases. In addition, interest in this research is due to the fact that the risk of HIV transmission is significantly higher during the acute phase. In the context of HIV infection, mathematical models play a crucial role in understanding disease dynamics, predicting outcomes, and informing treatment strategies. Evaluation of the parameters which characterized the model is essential for fitting the one to clinical data and improving our understanding of HIV infection pathogenesis.

Our mathematical model is based on consideration of a standard three-component model of the acute HIV infection dynamics, which describes, in terms of differential equations, the interaction of uninfected target cells, infected cells and viral particles. This model allows us to present a qualitative picture of the acute phase: a sharp increase in viral load, its peak and further decrease until the viral load is established at an equilibrium, and then calculate the basic rate of virus reproduction (R_0). The magnitude of R_0 ($R_0 = 1; < 1; > 1, \ll 1; \gg 1$) is an important flow indicator for HIV infections in the future.

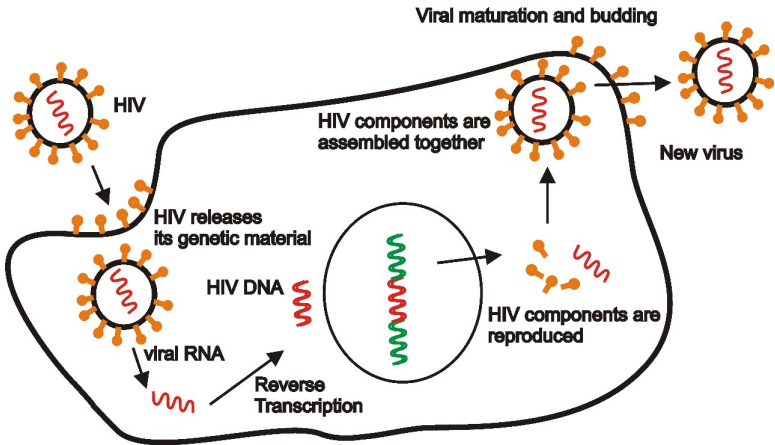


Figure 1: *The HIV life cycle.*

Our main contributions of this paper can be summarized as follows:

- Formulation of a novel immune response system of ODE which includes novel component integrated into the third equation of the classical three-equation HIV model, enhancing the biological realism of the system.
- Derivation of optimality conditions using a Lagrangian approach, leading to a complete numerical scheme for solving forward, adjoint, and parameter identification problems.
- Proof of three a posteriori error estimates to guide local time-mesh refinement and assess reconstruction accuracy.
- Introduction of an adaptive time-mesh refinement strategy that locally adjusts the time discretization based on residual analysis.
- Demonstration of method efficiency via clinical data, showing improved reconstruction of immune dynamics during the acute phase of HIV in four untreated patients.

The outline of the paper is as follows. The new mathematical model is proposed in section 2. The PIP is formulated in section 3. The Lagrangian approach and optimality conditions are derived in section 4. Numerical methods for solution of optimization problem are formulated in section 5. The a posteriori error estimates are derived in section 6: an a posteriori error estimate for the Tikhonov functional is formulated in section 6.1 and a posteriori error estimate for the error in the reconstructed immune response function is derived in section 6.2. Conjugate gradient algorithm (CGA) and adaptive conjugate gradient algorithm (ACGA) for solution of PIP are formulated in section 7. Finally, in section 8 numerical examples illustrate the effectiveness of the proposed ACGA using clinical data for four untreated HIV-infected patients taken from [5].

2 Description of the mathematical model

Recently in [1] was developed time-adaptive algorithm for determination of parameters in the mathematical model of HIV infection proposed in [2]. This model describes the effect of drug (Reverse Transcriptase Inhibitor, RTI) on the dynamics of HIV infection. Figure 1 presents the HIV life circle described by this model.

In the current work we consider the case of HIV-1 infection without treatment which will result in transformation of the system from [2] to three equations combined with the new component in the third equation.

Let us denote:

- $T(t)$ – population of uninfected target cells,
- $I(t)$ – population of infected target cells,
- $V(t)$ – population of viral particles,
- $E(t)$ – function that describes effectivity of immune response by CTLs (cytotoxic T-cells).

We also adjust the dimensions involved: mm^3 to ml and mm^{-3} to ml^{-1} , respectively, such that:

$$1 \text{ mm}^3 = 1 \mu\text{l} = 10^{-3} \text{ ml}, \quad 1 \text{ mm}^{-3} = 1 \mu\text{l}^{-1} = 10^3 \text{ ml}^{-1}.$$

Let us denote by $\Omega_t = [0, T_{obs}]$ the time domain for $t > 0$, where T_{obs} is the final observation time. The model problem considered in this works is:

$$\begin{cases} \frac{dT}{dt} = f_1(T(t), I(t), V(t), E(t)) = s - \beta_1 T(t)V(t) - \mu T(t), \\ \frac{dI}{dt} = f_2(T(t), I(t), V(t), E(t)) = \beta_1 T(t)V(t) - d(t)E(t)I(t), \\ \frac{dV}{dt} = f_3(T(t), I(t), V(t), E(t)) = \rho I(t) - \beta_2 T(t)V(t) - cV(t), \end{cases} \quad (2.1)$$

with initial conditions

$$T(0) = T^0 \text{ cell/ml}, \quad I(0) = I^0 \text{ cell/ml}, \quad V(0) = V^0 \text{ virion/ml}. \quad (2.2)$$

The parameters used in system (2.1) are described in Table 1.

To simplify notations for further analytical investigations we again use change of variables in system (2.1) as follows: $u_1(t) = T(t)$, $u_2(t) = I(t)$, $u_3(t) = V(t)$. Then the system (2.1) with

Parameter	Value	Units	Description
s	10^4	$cell/(ml \cdot day)$	inflow rate of T cells
μ	0.01	$1/day$	natural death rate of T cells
β_1	2.4e-8	$ml/(virion \cdot day)$	virus infectivity rate
β_2	2.4e-8	$ml/(cell \cdot day)$	rate of viral decline on infection of T-cells
d	0.26	$1/day$	death rate of infected cells
c	2.4	$1/day$	clearance rate of virus
ρ	10^3	$virion/(cell \cdot day)$	total number of viral particles produced by an infected cell

Table 1: Parameters dataset for system (2.1).

initial conditions (2.2) can be written for $t \in \Omega_t$ as

$$\begin{cases} \frac{du_1}{dt} = s - \beta_1 u_1(t)u_3(t) - \mu u_1(t), \\ \frac{du_2}{dt} = \beta_1 u_1(t)u_3(t) - d(t)E(t)u_2(t), \\ \frac{du_3}{dt} = \rho u_2(t) - \beta_2 u_1(t)u_3(t) - cu_3(t), \\ u_1(0) = u_1^0 \text{ cell/ml}, \\ u_2(0) = u_2^0 \text{ cell/ml}, \\ u_3(0) = u_3^0 \text{ virion/ml}. \end{cases} \quad (2.3)$$

Figure 2 shows schematic behaviour of interactions between HIV and T-cells described by system (2.3).

The problem (2.3) can be presented in the following compact form:

$$\begin{cases} \frac{du}{dt} = f(u(t), E(t)) & t \in \Omega_t, \\ u(0) = u^0, \end{cases} \quad (2.4)$$

where all involved functions are denoted as

$$\begin{aligned} u &= u(t) = (u_1(t), u_2(t), u_3(t))^T, \\ u^0 &= (u_1(0), u_2(0), u_3(0))^T, \\ \frac{du}{dt} &= \left(\frac{\partial u_1}{\partial t}, \frac{\partial u_2}{\partial t}, \frac{\partial u_3}{\partial t} \right)^T, \\ f(u(t), E(t)) &= (f_1, f_2, f_3)^T(u(t), E(t)) = \\ &= (f_1(u_1, u_2, u_3, E(t)), \dots, f_3(u_1, u_2, u_3, E(t)))^T. \end{aligned} \quad (2.5)$$

Here, $(\cdot)^T$ denotes transposition operator.

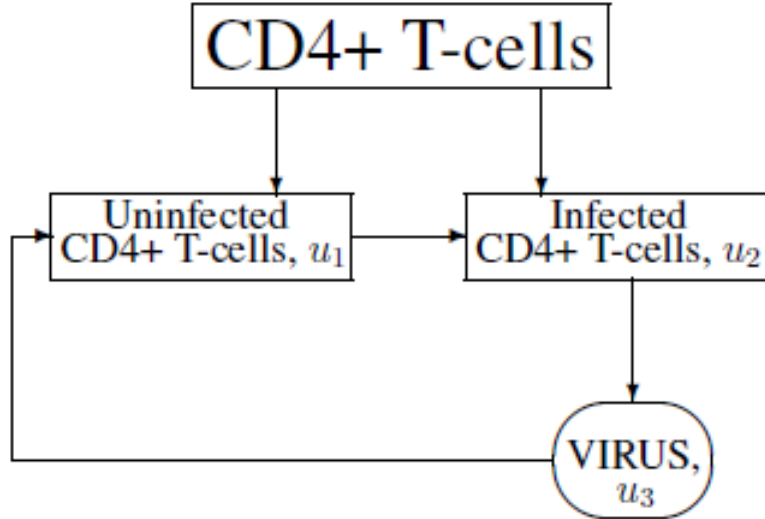


Figure 2: *Interaction between HIV and T-cells.*

In the current work we are interesting in the development of time-adaptive algorithm for determination of the function $E(t)$ in system (2.3) using clinical data of four patients taken from [5]. The function $E(t)$ describes effectiveness of immune response during treatment of HIV infection. Determination of this parameter is very important for doctors for analysis of each treated patient since according to [6], a single HIV-1 infected cell produces between 10^3 and more than 10^4 viral particles over its life span. In the work [5] (see Fig. 1-b) in [5]) clinical data for the function $V(T)$ – viral load in the plasma – and the function $\Sigma = T(t) + I(t)$ – total CD4+ T cell count – are presented for four patients with HIV without treatment. Data were measured during one year period of the hyperacute and acute HIV infection in the 8 points (pre-infection, 0 weeks, 1 weeks, 2 weeks, 3 weeks, 4 weeks, 6 months, 1 year). Table 2 and Table 3 summarize the clinical data.

N point	$\log_{10} V(t)$ $\text{copies} \cdot ml^{-1}$	$\Sigma = T(t) + I(t)$ $\times 10^3 \text{ cells} \cdot ml^{-1}$	N point	$\log_{10} V(t)$ $\text{copies} \cdot ml^{-1}$	$\Sigma = T(t) + I(t)$ $\times 10^3 \text{ cells} \cdot ml^{-1}$
1.	0.0	1125.	1.	0.0	750.
2.	5.5	825.	2.	5.5	630.
3.	7.75	675.	3.	7.0	450.
4.	6.5	525.	4.	5.75	280.
5.	5.5	540.	5.	4.8	750.
6.	5.3	525.	6.	3.8	570.
7.	4.5	550.	7.	4.3	450.
8.	5.1	600.	8.	4.0	530.

Patient 1

Patient 2

Table 2: Clinical data corresponding to Fig. 1-b of [6].

N point	$\log_{10} V(t)$ $\text{copies} \cdot ml^{-1}$	$\Sigma = T(t) + I(t)$ $\times 10^3 \text{ cells} \cdot ml^{-1}$	N point	$\log_{10} V(t)$ $\text{copies} \cdot ml^{-1}$	$\Sigma = T(t) + I(t)$ $\times 10^3 \text{ cells} \cdot ml^{-1}$
1.	0.0	700.	1.	0.0	615.
2.	5.7	430.	2.	3.7	700.
3.	7.4	300.	3.	5.7	450.
4.	6.8	480.	4.	6.	615.
5.	4.2	570.	5.	3.9	575.
6.	3.8	450.	6.	3.5	520.
7.	3.2	630.	7.	3.	450.
8.	3.7	510.	8.	3.	615.

Patient 3

Patient 4

Table 3: Clinical data corresponding to Fig. 1-b of [6].

To proceed further we introduce several mathematical assumptions which are necessary for development of a stable reconstruction algorithm. First, we assume that in the system (2.4) the function $f \in C^1(\Omega_t)$ is Lipschitz continuous. Next, accordingly to work [30] we assume that the function $E(t) \in C(\Omega_t)$ belongs to the following set of admissible parameters M_E :

$$M_E = \{E(t) \in C(\Omega_t) : E(t) \in [1, 10] \text{ in } \Omega_t\}. \quad (2.6)$$

3 The parameter identification problem

To formulate the parameter identification problem we assume that all parameters in system (2.4) are known except the control parameter $E(t)$ which presents time-dependent distribution of viral particles produced by one infected cell. The values of other parameters $\{s, \mu, \beta, \rho, c\}$, and $d(t) = d$ in the model (2.4) correspond to values in the Table 1. We note that though in the Table 1 the death rate function of infected T-cells $d(t)$ is defined as a constant, i.e., $d(t) = d$, in numerical experiments we take the function $d(t)$ as a time-dependent function of a special form - see more details in section 8.

Parameter Identification Problem (PIP). Assume that the condition (2.6) for the function $E(t)$ holds and parameters $\{s, \mu, \beta_1, \beta_2, d, \rho, c\}$ in system (2.4) are known. Assume further that the

function $E(t) \in M_E$ is unknown inside the domain Ω_t . The PIP is: determine $E(t)$ for $t \in \Omega_t$, under the conditions that the population function $g_1(t)$ of total number of the uninfected and infected T cells is known:

$$u_1(t) + u_2(t) \approx g_1(t), \quad t \in \Omega_t, \quad (3.7)$$

as well as the virus population function $g_2(t)$ is known:

$$u_3(t) \approx g_2(t), \quad t \in \Omega_t. \quad (3.8)$$

Here, the function $g_1(t)$ presents observations of the sum $u_1(t) + u_2(t)$, or uninfected and infected T cells, and $g_2(t)$ presents observations of the virus function $u_3(t)$ over the domain Ω_t .

4 Optimization method

Let H be a Hilbert space of functions defined in Ω_t . To determine $E(t)$, $t \in \Omega_t$, we construct the Tikhonov functional which is more appropriate for the data presented in Tables 2 and 3:

$$\begin{aligned} J(E) = & \frac{1}{2} \int_{\Omega_t} [\log_{10}(u_1(t) + u_2(t)) - \log_{10}(g_1(t))]^2 z_{1\zeta}(t) dt \\ & + \frac{1}{2} \int_{\Omega_t} [\log_{10} u_3(t) - \log_{10} g_2(t)]^2 z_{2\zeta}(t) dt + \frac{1}{2} \gamma \int_{\Omega_t} (E(t) - E^0)^2 dt. \end{aligned} \quad (4.9)$$

Here, $u_1(t)$, $u_2(t)$, $u_3(t)$ are the solutions of the system (2.4) which are depended on the function $E(t)$, $g_1(t)$ is the observed sum of uninfected and infected T-cells, $g_2(t)$ is the observed virus population function, E^0 is the initial guess for the parameter $E(t)$ and $\gamma \in (0, 1)$ is the regularization parameter, $z_{1\zeta}(t)$, $\zeta \in (0, 1)$ and $z_{2\zeta}(t)$, $\zeta \in (0, 1)$ are smoothing functions for data which can be defined similarly as in [13].

To find the function $E(t) \in H$ which minimizes the Tikhonov functional (4.9) we seek for a stationary point of (4.9) with respect to E such that

$$J'(E)(\bar{E}) = 0, \quad \forall \bar{E} \in H. \quad (4.10)$$

To find minimum of (4.9) we use constrained optimization with the standard Lagrangian approach [8, 27] and introduce the Lagrangian with constraints corresponding to the model problem:

$$L(v) = J(E) + \sum_{i=1}^3 \int_{\Omega_t} \lambda_i \left(\frac{du_i}{dt} - f_i \right) dt, \quad (4.11)$$

where $u(t) = (u_1(t), u_2(t), u_3(t))$ is the solution of the system (2.4), $\lambda(t)$ is the vector of Lagrange multipliers $\lambda(t) = (\lambda_1(t), \lambda_2(t), \lambda_3(t))$, and $v = (\lambda, u, E)$.

We now introduce following spaces which we are using in analysis of PIP:

$$\begin{aligned} H_u^1(\Omega_t) &= \{u \in H^1(\Omega_t) : u(0) = u_0\}, \\ H_\lambda^1(\Omega_t) &= \{\lambda \in H^1(\Omega_t) : \lambda(T) = 0\}, \\ U &= H_u^1(\Omega_t) \times H_\lambda^1(\Omega_t) \times C(\Omega_t), \end{aligned} \quad (4.12)$$

for all real valued functions.

To derive the Fréchet derivative of the Lagrangian (4.11) we use such called all-at-once approach when we assume that functions $v = (\lambda, u, E)$ can be varied independently of each other such that

$$L'(v)(\bar{v}) = 0, \quad \forall \bar{v} = (\bar{\lambda}, \bar{u}, \bar{E}) \in U. \quad (4.13)$$

The optimality condition (4.13) means also that for all $\bar{v} \in U$ we have

$$L'(v; \bar{v}) = \frac{\partial L}{\partial \lambda}(v)(\bar{\lambda}) + \frac{\partial L}{\partial u}(v)(\bar{u}) + \frac{\partial L}{\partial E}(v)(\bar{E}) = 0 \quad (4.14)$$

i.e., every component of (4.14) should be zero out. Thus, the optimality condition $\frac{\partial L}{\partial \lambda}(v)(\bar{\lambda}) = 0$ yields

$$\begin{aligned} 0 &= \frac{\partial L}{\partial \lambda_1}(v)(\bar{\lambda}_1) = \int_{\Omega_t} \left(\frac{\partial u_1}{\partial t} - s + \beta_1 u_1 u_3 + \mu u_1 \right) \bar{\lambda}_1 dt \quad \forall \bar{\lambda}_1 \in H_\lambda^1(\Omega_t), \\ 0 &= \frac{\partial L}{\partial \lambda_2}(v)(\bar{\lambda}_2) = \int_{\Omega_t} \left(\frac{\partial u_2}{\partial t} - \beta_1 u_1 u_3 + dE u_2 \right) \bar{\lambda}_2 dt, \quad \forall \bar{\lambda}_2 \in H_\lambda^1(\Omega_t) \\ 0 &= \frac{\partial L}{\partial \lambda_3}(v)(\bar{\lambda}_3) = \int_{\Omega_t} \left(\frac{\partial u_3}{\partial t} - \rho u_2 + c u_3 + \beta_2 u_1 u_3 \right) \bar{\lambda}_3 dt, \quad \forall \bar{\lambda}_3 \in H_\lambda^1(\Omega_t), \end{aligned} \quad (4.15)$$

Next, the optimality condition $\frac{\partial L}{\partial u}(v)(\bar{u}) = 0$ means that

$$\begin{aligned} 0 &= \frac{\partial L}{\partial u_1}(v)(\bar{u}_1) = \int_{\Omega_t} \frac{1}{(u_1 + u_2) \ln 10} [\log_{10}(u_1(t) + u_2(t)) - \log_{10}(g_1(t))] z_{1\zeta}(t) \bar{u}_1 dt \\ &\quad + \int_{\Omega_t} \left(-\frac{\partial \lambda_1}{\partial t} + \lambda_1 \beta_1 u_3 + \mu \lambda_1 - \lambda_2 \beta_1 u_3 + \beta_2 \lambda_3 u_3 \right) \bar{u}_1 dt \quad \forall \bar{u}_1 \in H_u^1(\Omega_t), \\ 0 &= \frac{\partial L}{\partial u_2}(v)(\bar{u}_2) = \int_{\Omega_t} \frac{1}{(u_1 + u_2) \ln 10} [\log_{10}(u_1(t) + u_2(t)) - \log_{10}(g_1(t))] z_{1\zeta}(t) \bar{u}_2 dt \\ &\quad + \int_{\Omega_t} \left(-\frac{\partial \lambda_2}{\partial t} + dE \lambda_2 - \lambda_3 \rho \right) \bar{u}_2 dt \quad \forall \bar{u}_2 \in H_u^1(\Omega_t), \\ 0 &= \frac{\partial L}{\partial u_3}(v)(\bar{u}_3) = \int_{\Omega_t} \frac{1}{u_3 \ln 10} [\log_{10}(u_3) - \log_{10}(g_2)] z_{1\zeta}(t) \bar{u}_3 dt \\ &\quad + \int_{\Omega_t} \left(-\frac{\partial \lambda_3}{\partial t} + \lambda_1 \beta_1 u_1 - \lambda_2 \beta_1 u_1 + c \lambda_3 + \lambda_3 \beta_2 u_1 \right) \bar{u}_3 dt \quad \forall \bar{u}_3 \in H_u^1(\Omega_t). \end{aligned} \quad (4.16)$$

Finally, the optimality condition $\frac{\partial L}{\partial E}(v)(\bar{E}) = 0$ yields:

$$0 = \frac{\partial L}{\partial E}(v)(\bar{E}) = \gamma \int_{\Omega_t} (E - E^0) \bar{E} dt + \int_{\Omega_t} d\lambda_2 u_2 \bar{E} dt \quad \forall \bar{E} \in C(\Omega_t). \quad (4.17)$$

Using optimality conditions (4.15)-(4.16) we observe that the equations (4.15) correspond to the system of model equations (2.3) which is also our forward problem, and equations (4.16) — to the following adjoint problem

$$\begin{aligned} \frac{\partial \lambda_1}{\partial t} &= \tilde{f}_1(\lambda(t), \eta(t)) = \lambda_1(t)\beta_1 u_3(t) + \lambda_1(t)\mu - \lambda_2(t)\beta_1 u_3(t) + \beta_2 \lambda_3(t)u_3(t) \\ &\quad + \frac{1}{(u_1(t) + u_2(t)) \ln 10} [\log_{10}(u_1(t) + u_2(t)) - \log_{10}(g_1)]z_{1\zeta}, \\ \frac{\partial \lambda_2}{\partial t} &= \tilde{f}_2(\lambda(t), \eta(t)) = -\lambda_3(t)\rho + d\lambda_2(t)E(t) \\ &\quad + \frac{1}{(u_1(t) + u_2(t)) \ln 10} [\log_{10}(u_1(t) + u_2(t)) - \log_{10}(g_1)]z_{1\zeta}, \quad (4.18) \\ \frac{\partial \lambda_3}{\partial t} &= \tilde{f}_3(\lambda(t), \eta(t)) = \lambda_1(t)\beta_1 u_1(t) - \lambda_2(t)\beta_1 u_1(t) + c\lambda_3(t) + \lambda_3(t)\beta_2 u_1(t) \\ &\quad + \frac{1}{u_3(t) \ln 10} [\log_{10}(u_3(t)) - \log_{10}(g_2)]z_{1\zeta}, \\ \lambda_i(T) &= 0, \quad i = 1, 2, 3, \end{aligned}$$

which we rewrite as

$$\begin{cases} \frac{\partial \lambda}{\partial t} = \tilde{f}(\lambda(t), E(t)), \\ \lambda_i(T) = 0, \quad i = 1, 2, 3, \end{cases} \quad (4.19)$$

with

$$\begin{aligned} \lambda &= \lambda(t) = (\lambda_1(t), \lambda_2(t), \lambda_3(t))^T, \\ 0 &= (\lambda_1(T), \lambda_2(T), \lambda_3(T))^T, \\ \frac{d\lambda}{dt} &= \left(\frac{\partial \lambda_1}{\partial t}, \frac{\partial \lambda_2}{\partial t}, \frac{\partial \lambda_3}{\partial t} \right)^T, \quad (4.20) \\ \tilde{f}(\lambda(t)) &= (\tilde{f}_1, \tilde{f}_2, \tilde{f}_3)(\lambda(t), E(t))^T. \end{aligned}$$

The adjoint problem should be solved backwards in time with already known forward problem solution $u(t)$ and a given data $g_1(t), g_2(t)$.

From definition of the Lagrangian (4.11) it follows that for the known exact function u , known parameters in the forward problem and known solution λ of the adjoint problem (4.18) we get that

$$L(v(E)) = J(E). \quad (4.21)$$

In this case the Fréchet derivative of the Tikhonov functional can be written as

$$J'(E) := J_E(u(E), E) = \frac{\partial J}{\partial E}(u(E), E) = \frac{\partial L}{\partial E}(v(E)). \quad (4.22)$$

Using (4.17) in (4.22), we get the following expression for the Fréchet derivative of the Tikhonov functional which will be used later in the conjugate gradient update of the parameter E in time :

$$J'(E)(t) = \gamma(E - E^0)(t) + d\lambda_2(t)u_2(t). \quad (4.23)$$

5 Numerical methods for solution of optimization problem

To solve the minimization problem (4.13) we will employ the finite element method. To do this we discretize the computational domain $\Omega_t = [0, T]$ and consider a partition $J_\tau = \{J_k\}$ of the time domain Ω_t into time subintervals $J_k = (t_{k-1}, t_k]$ with the time step $\tau_k = t_k - t_{k-1}$. Let us define the piecewise-constant function $\tau(t)$ such that

$$\tau(t) = \tau_k, \quad \forall J_k \in J_\tau. \quad (5.24)$$

We define also the finite element spaces $V_\tau^u \subset H_u^1(\Omega_t)$ and $V_\tau^\lambda \subset H_\lambda^1(\Omega_t)$ for approximations u_τ, λ_τ of u and λ , respectively, as

$$\begin{aligned} V_\tau^u &= \{u \in L_2(\Omega_t) : u|_J \in P^0(J), u(0) = u^0, \quad \forall J \in J_\tau\}, \\ V_\tau^\lambda &= \{\lambda \in L_2(\Omega_t) : \lambda|_J \in P^0(J), \lambda(T) = 0, \quad \forall J \in J_\tau\} \end{aligned} \quad (5.25)$$

for discretization of the state and adjoint problems. We also introduce the finite element space $V_\tau^E \subset L_2(\Omega_t)$ for the function $E(t)$ consisting of piecewise constant functions

$$V_\tau^E = \{f \in L_2(\Omega_t) : f|_J \in P^0(J) \quad \forall J \in J_\tau\}. \quad (5.26)$$

Let $U_\tau = V_\tau^u \times V_\tau^\lambda \times V_\tau^E$ such that $U_\tau \subset U$. We can formulate now the finite element method for (4.13): find $v_\tau \in U_\tau$ such that

$$L'(v_\tau)(\bar{v}) = 0, \quad \forall \bar{v} \in U_\tau. \quad (5.27)$$

We note that the forward (2.3) and adjoint (4.18) problems are nonlinear. For solution of these problems we employ Newton's method as follows. The variational formulation of the forward problem (2.4) is:

$$\left(\frac{du}{dt}, \bar{u} \right) = (f(u(t)), \bar{u}) \quad \forall \bar{u} \in H_u^1(\Omega_t). \quad (5.28)$$

Let us use the following discretization for the derivative in time

$$\frac{\partial u}{\partial t} = \frac{u^{k+1} - u^k}{\tau_k}$$

in the variational formulation (5.28) to obtain

$$(u^{k+1}, \bar{u}) - \tau_k(f(u^{k+1}), \bar{u}) - (u^k, \bar{u}) = 0 \quad \forall \bar{u} \in H_u^1(\Omega_t). \quad (5.29)$$

Approximating u^{k+1} by its finite element approximation u_τ^{k+1} the above equation can be written as

$$(u_\tau^{k+1} - \tau_k f(u_\tau^{k+1}) - u_\tau^k, \bar{u}) = 0 \quad \forall \bar{u} \in V_\tau^u. \quad (5.30)$$

We denote now

$$\begin{aligned} \tilde{u} &= u_\tau^{k+1}, \\ V(\tilde{u}) &= \tilde{u} - \tau_k f(\tilde{u}) - u_\tau^k. \end{aligned} \quad (5.31)$$

Next, we rewrite the variational formulation as

$$(V(\tilde{u}), \bar{u}) = 0 \quad \forall \bar{u} \in V_\tau^u. \quad (5.32)$$

To solve nonlinear equation $V(\tilde{u}) = 0$ we are using the Newton's method [17] for iterations in the Newtons' method $n = 1, \dots, M_n$:

$$\tilde{u}^{n+1} = \tilde{u}^n - [V'(\tilde{u}^n)]^{-1} \cdot V(\tilde{u}^n). \quad (5.33)$$

Here, the Jacobian $V'(\tilde{u}^n)$ is computed via definition of $V(\tilde{u})$ in (5.31) as

$$V'(\tilde{u}^n) = I - \tau_k f'(\tilde{u}^n),$$

where I is the identity matrix, $f'(\tilde{u}^n)$ is the Jacobian of f which represents the right hand side of the forward problem (2.3) at \tilde{u}^n , n is the iteration number in Newton's method and M_n is the final iteration in Newton's method. The entries in the Jacobian $f'(\tilde{u}^n)$ for system (2.3) can be explicitly computed and they are defined as:

$$f'(\tilde{u}^n) = \begin{bmatrix} \frac{\partial f_1}{\partial u_1} & \frac{\partial f_1}{\partial u_2} & \frac{\partial f_1}{\partial u_3} \\ \frac{\partial f_2}{\partial u_1} & \frac{\partial f_2}{\partial u_2} & \frac{\partial f_2}{\partial u_3} \\ \frac{\partial f_3}{\partial u_1} & \frac{\partial f_3}{\partial u_2} & \frac{\partial f_3}{\partial u_3} \end{bmatrix} (\tilde{u}^n) = \begin{bmatrix} -\beta_1 u_{3\tau}^n - \mu & 0 & -\beta_1 u_{1\tau}^n \\ \beta_1 u_{3\tau}^n & -d E & \beta_1 u_{1\tau}^n \\ -\beta_2 u_{3\tau}^n & \rho & -\beta_2 u_{1\tau}^n - c \end{bmatrix}.$$

We derive the Newtons's method for the solution the adjoint problem (4.18) in a similar way. Since we solve the adjoint problem backwards in time starting from the known $\lambda(T) = 0$, we discretize the time derivative as

$$\frac{\partial \lambda}{\partial t} = \frac{\lambda^{k+1} - \lambda^k}{\tau_k} \quad (5.34)$$

for the already known λ^{k+1} , and write the variational formulation of the adjoint problem for all $\bar{\lambda} \in H_\lambda^1(\Omega_t)$ as

$$(\lambda^{k+1} - \lambda^k - \tau_k \tilde{f}(\lambda^k), \bar{\lambda}) = 0. \quad (5.35)$$

We rewrite (5.35) in the form

$$(\lambda^k - \lambda^{k+1} + \tau_k \tilde{f}(\lambda^k), \bar{\lambda}) = 0 \quad (5.36)$$

and formulate the finite element method for the variational formulation (5.36): find $\lambda_\tau^k \in V_\tau^\lambda$ such that for all $\bar{\lambda} \in V_\tau^\lambda$

$$(\lambda_\tau^k - \lambda_\tau^{k+1} + \tau_k \tilde{f}(\lambda_\tau^k), \bar{\lambda}) = 0. \quad (5.37)$$

Denoting

$$\begin{aligned} \tilde{\lambda} &= \lambda_\tau^k, \\ R(\tilde{\lambda}) &= \tilde{\lambda} + \tau_k \tilde{f}(\tilde{\lambda}) - \lambda_\tau^{k+1}, \end{aligned} \quad (5.38)$$

we can rewrite (5.37) for all $\bar{\lambda} \in V_\tau^\lambda$ as

$$(R(\tilde{\lambda}), \bar{\lambda}) = 0. \quad (5.39)$$

For solution $R(\tilde{\lambda}) = 0$ we use again Newton's method:

$$\tilde{\lambda}^{n+1} = \tilde{\lambda}^n - [R'(\tilde{\lambda}^n)]^{-1} \cdot R(\tilde{\lambda}^n), n = 1, \dots, K_n. \quad (5.40)$$

We compute $R'(\tilde{\lambda}^n)$ using the definition of $R(\tilde{\lambda})$ in (5.38) as

$$R'(\tilde{\lambda}^n) = I + \tau_k \tilde{f}'(\tilde{\lambda}^n),$$

where I is the identity matrix, $\tilde{f}'(\tilde{\lambda}^n)$ is the Jacobian of \tilde{f} at $\tilde{\lambda}^n$, n is the iteration number in the Newton's method and K_n is the final number of iteration. The entries in the Jacobian $\tilde{f}'(\tilde{\lambda}^n)$ for the adjoint system (4.18) are explicitly given by

$$\tilde{f}'(\tilde{\lambda}^n) = \begin{bmatrix} \frac{\partial \tilde{f}_1}{\partial \lambda_1} & \frac{\partial \tilde{f}_1}{\partial \lambda_2} & \frac{\partial \tilde{f}_1}{\partial \lambda_3} \\ \frac{\partial \tilde{f}_2}{\partial \lambda_1} & \frac{\partial \tilde{f}_2}{\partial \lambda_2} & \frac{\partial \tilde{f}_2}{\partial \lambda_3} \\ \frac{\partial \tilde{f}_3}{\partial \lambda_1} & \frac{\partial \tilde{f}_3}{\partial \lambda_2} & \frac{\partial \tilde{f}_3}{\partial \lambda_3} \end{bmatrix} (\tilde{\lambda}^n) = \begin{bmatrix} \beta_1 u_{3\tau}^n + \mu & -\beta_1 u_{3\tau}^n & \beta_2 u_{3\tau}^n \\ 0 & dE & -\rho \\ \beta_1 u_{1\tau}^n & -\beta_1 u_{1\tau}^n & c + \beta_2 u_{1\tau}^n \end{bmatrix}.$$

We note that $\det f'(\tilde{u}^n) \neq 0$ as well as $\det \tilde{f}'(\tilde{\lambda}^n) \neq 0$ since all parameters used in the model problem are non-zero. Thus, schemes given by formulas (5.33), (5.40) will converge to the solutions of forward and adjoint problems for the appropriate initial guesses for values \tilde{u}^1 and $\tilde{\lambda}^1$, correspondingly.

6 A Posteriori Error Estimates

In this section we derive a posteriori error estimates for the error in The Tikhonov's functional $\|J(E) - J(E_h)\|_{L_2(\Omega_t)}$ and for the error in the reconstructed function $\|E - E_h\|_{L_2(\Omega_t)}$, correspondingly. Both error estimators can be used as the mesh refinement criteriors in the adaptive conjugate gradient algorithm.

Before deriving error estimates we make some assumptions which are usual for parameter identification problems since they are ill-posed problems [35, 36, 37]. We assume that the function $E(t) \in C(\Omega_t)$ as a minimizer of the Lagrangian (4.11), and $E_\tau \in V_\tau^E$ is its finite element approximation. We also assume that $E^* \in C(\Omega_t)$ is the exact function describing the effectivity of the immune response and that there exists a good approximation E_τ to the exact function $E^* \in C(\Omega_t)$. Let $g_{1,2}^*(t)$ be the exact data for the measured functions $g_{1,2}(t)$ defined in (3.7), (3.8), correspondingly, and the functions $g_{1,2\sigma}(t)$ represent the error levels in the measured data. This means that we assume that measurements $g_{1,2}(t)$ in (3.7), (3.8) are given with some small noise levels σ_1, σ_2 such that

$$\begin{aligned} g_1(t) &= g_1^*(t) + g_{1\sigma}(t); \quad g_1^*, g_{1\sigma} \in L_2(\Omega_t), \quad \|g_{1\sigma}\|_{L_2(\Omega_t)} \leq \sigma_1, \\ g_2(t) &= g_2^*(t) + g_{2\sigma}(t); \quad g_2^*, g_{2\sigma} \in L_2(\Omega_t), \quad \|g_{2\sigma}\|_{L_2(\Omega_t)} \leq \sigma_2. \end{aligned} \quad (6.41)$$

We also assume that the regularization parameter in the Tikhonov's functional is such that

$$\gamma = \gamma(\sigma_1, \sigma_2) = (\sigma_1 + \sigma_2)^{2\mu}, \quad \mu \in (0, 1/4), \quad \sigma_{1,2} \in (0, 1) \quad (6.42)$$

and for the exact solution E^* corresponding to the exact data $g_{1,2}^*(t)$ it holds that

$$\|E_0 - E^*\|_{L_2(\Omega_t)} \leq \frac{(\sigma_1 + \sigma_2)^{3\mu}}{3}. \quad (6.43)$$

The condition (6.43) means that E_0 is located in the close neighborhood of the exact solution E^* .

Let us define the set for any $\varepsilon > 0$

$$V_\varepsilon(E) = \{\tilde{E} \in C(\Omega_t) : \|E - \tilde{E}\| < \varepsilon \quad \forall E \in C(\Omega_t)\}. \quad (6.44)$$

Assume that for all $E \in V_1(E^*)$ the operator

$$\begin{aligned} F(E) = & \frac{1}{2} \int_{\Omega_t} [\log_{10}(u_1(E, t) + u_2(E, t)) - \log_{10}(g_1(t))]^2 z_{1\zeta}(t) \, dt \\ & + \frac{1}{2} \int_{\Omega_t} [\log_{10} u_3(E, t) - \log_{10} g_2(t)]^2 z_{2\zeta}(t) \, dt \end{aligned}$$

has the Fréchet derivative $F'(E)$ which is bounded and Lipschitz continuous in $V_1(E^*)$ for $N_1, N_2 = \text{const.} > 0$

$$\begin{aligned} \|F'(E)\|_{L_2(\Omega_t)} &\leq N_1 \quad \forall E \in V_1(E^*), \\ \|F'(E_1) - F'(E_2)\|_{L_2(\Omega_t)} &\leq N_2 \|E_1 - E_2\|_{L_2(\Omega_t)} \quad \forall E_1, E_2 \in V_1(E^*). \end{aligned} \quad (6.45)$$

6.1 An a posteriori error estimate for the Tikhonov functional

In this section we derive an a posteriori error estimate for the error $\|J(E) - J(E_h)\|_{L_2(\Omega_t)}$ in the Tikhonov functional (4.9) on the finite element time partition J_τ .

Theorem 1. *Let $E \in C(\Omega_t)$ is the minimizer of the functional $J(E)$ defined by (4.9) and there exists finite element approximation of a minimizer $E_\tau \in V_\tau^E$ of $J(E)$. Then the following a posteriori error estimate for the error $e = \|J(E) - J(E_\tau)\|_{L^2(\Omega_t)}$ in the Tikhonov functional (4.9) holds true*

$$e = \|J(E) - J(E_\tau)\|_{L^2(\Omega_t)} \leq C_I \|J'(E_\tau)\|_{L^2(\Omega_t)} \left(\|\tau E_\tau\|_{L_2(\Omega_t)} + \sum_{J_k} \| [E_\tau] \|_{L_2(J_k)} \right) \quad \forall E_\tau \in V_\tau^E, \quad (6.46)$$

where $C_I = \text{const.} > 0$ and

$$J'(E_\tau) = \gamma(E_\tau - E^0) + d\lambda_{2\tau} u_{2\tau}. \quad (6.47)$$

Proof Using first two terms in the Taylor's expansion we get

$$J(E) = J(E_\tau) + J'(E_\tau)(E - E_\tau) + R(E, E_\tau), \quad (6.48)$$

where $R(E, E_\tau) = O(\|E - E_\tau\|^2)$, $(E - E_\tau) \rightarrow 0 \quad \forall E, E_\tau \in V_\tau^E$. We neglect the remainder term $R(E, E_\tau)$ in (6.48) since it is small because of assumption (6.43). Next, we use the following splitting for $E - E_\tau$ in (6.48)

$$E - E_\tau = E - E_\tau^I + E_\tau^I - E_\tau \quad (6.49)$$

together with the Galerkin orthogonality property

$$J'(E_\tau)(E_\tau^I - E_\tau) = 0, \quad \forall E_\tau^I, E_\tau \in V_\tau^E \quad (6.50)$$

to get

$$J(E) - J(E_\tau) \leq J'(E_\tau)(E - E_\tau^I). \quad (6.51)$$

Here, E_τ^I is a standard interpolant of E on the mesh J_τ [21]. Taking norms in (6.51), we obtain

$$\|J(E) - J(E_\tau)\|_{L^2(\Omega_t)} \leq \|J'(E_\tau)\|_{L^2(\Omega_t)} \|E - E_\tau^I\|_{L^2(\Omega_t)}. \quad (6.52)$$

For estimation of the term $\|E - E_\tau^I\|_{L^2(\Omega_t)}$ we are using standard interpolation estimate with the interpolation constant C_I

$$\|E - E_\tau^I\|_{L^2(\Omega_t)} \leq C_I \|\tau E\|_{H^1(\Omega_t)}. \quad (6.53)$$

We can estimate $\|\tau E\|_{H^1(\Omega_t)}$ in (6.53) as

$$\begin{aligned} \|\tau E\|_{H^1(\Omega_t)} &\leq \sum_{J_k} \|\tau_k E\|_{H^1(J_k)} = \sum_{J_k} \left\| \left(E + \frac{\partial E}{\partial t} \right) \tau_k \right\|_{L_2(J_k)} \\ &\leq \sum_{J_k} \left(\|E_\tau \tau_k\|_{L_2(J_k)} + \left\| \frac{[E_\tau]}{\tau_k} \tau_k \right\|_{L_2(J_k)} \right) \\ &\leq \|\tau E_\tau\|_{L_2(\Omega_t)} + \sum_{J_k} \|[E_\tau]\|_{L_2(J_k)}. \end{aligned} \quad (6.54)$$

Here, $[E_\tau]$ denote the jump of the function E_τ over the time intervals $[t_{k-1}, t_k]$ and $[t_k, t_{k+1}]$ which we define as

$$[E_\tau] = E_\tau^+ - E_\tau^-,$$

where functions E_τ^-, E_τ^+ are computed on two neighboring time intervals $[t_{k-1}, t_k]$ and $[t_k, t_{k+1}]$, respectively.

Now we substitute the estimate (6.54) into (6.52) to get final a posteriori error estimate

$$\|J(E) - J(E_\tau)\|_{L^2(\Omega_t)} \leq C_I \|J'(E_\tau)\|_{L^2(\Omega_t)} \left(\|\tau E_\tau\|_{L_2(\Omega_t)} + \sum_{J_k} \|[E_\tau]\|_{L_2(J_k)} \right) \quad \forall E_\tau \in V_\tau^E. \quad (6.55)$$

□

6.2 A posteriori error estimate of the minimizer on refined meshes

In the Theorem 2 and Theorem 3 we derive two different a posteriori error estimates for the error $\|E - E_\tau\|_{L^2(\Omega_t)}$. Proof of the Theorem 2 follows from the proof of Theorem 5.1 of [23].

Theorem 2

Let $E \in L^2(\Omega_t)$ be a minimizer of the Tikhonov's functional (4.9) and $E_\tau \in V_\tau^E$ be a finite element approximation of the minimizer on the finite element mesh J_τ . Then there exists a Lipschitz constant $D = \text{const.} > 0$ defined by

$$\|J'(E_1) - J'(E_2)\|_{L_2(\Omega_t)} \leq D \|E_1 - E_2\|_{L_2(\Omega_t)}, \quad \forall E_1, E_2 \in L_2(\Omega_t), \quad (6.56)$$

and the interpolation constant C_I independent on the mesh size τ such that the following a posteriori error estimate for the minimizer E holds true for $\gamma > 0$

$$\|E - E_\tau\|_{L_2(\Omega_t)} \leq \frac{D}{\gamma} C_I \left(\|\tau E_\tau\|_{L_2(\Omega_t)} + \sum_{J_k} \|[\tau E_\tau]\|_{L_2(J_k)} \right) \quad \forall E_\tau \in V_\tau^E. \quad (6.57)$$

Proof.

Let E_τ be the minimizer of the Tikhonov functional (4.9). The existence and uniqueness of this minimizer is guaranteed by conditions (6.43) and thus follows from Theorem 1.9.1.2 of [14]. Using this theorem we can conclude that the functional (4.9) is strongly convex on the space $L_2(\Omega_t)$ with the strong convexity constant γ . This yields that

$$\gamma \|E - E_\tau\|_{L_2(\Omega_t)}^2 \leq \| (J'(E) - J'(E_\tau), E - E_\tau) \|_{L_2(\Omega_t)}. \quad (6.58)$$

Here, $J'(E_\tau)$, $J'(E)$ are the Fréchet derivatives of the functional (4.9) given by the formula (4.23) for E_τ , E , respectively.

Since E is the minimizer of the Tikhonov functional (4.9) then

$$(J'(E), v) = 0, \quad \forall v \in L_2(\Omega_t).$$

Using again the splitting (6.49) in (6.58) together with the Galerkin orthogonality principle for all $E_\tau, E_\tau^I \in V_\tau^E$

$$(J'(E) - J'(E_\tau), E_\tau^I - E_\tau) = 0 \quad (6.59)$$

we get

$$\gamma \|E - E_\tau\|_{L_2(\Omega_t)}^2 \leq \| (J'(E) - J'(E_\tau), E - E_\tau^I) \|_{L_2(\Omega_t)}. \quad (6.60)$$

We can estimate the right hand side of (6.60) using (6.56) as

$$\| (J'(E) - J'(E_\tau), E - E_\tau^I) \|_{L_2(\Omega_t)} \leq D \|E - E_\tau\|_{L_2(\Omega_t)} \|E - E_\tau^I\|_{L_2(\Omega_t)}.$$

Substituting above equation into (6.60) we obtain

$$\|E - E_\tau\|_{L_2(\Omega_t)} \leq \frac{D}{\gamma} \|E - E_\tau^I\|_{L_2(\Omega_t)}. \quad (6.61)$$

Using again the interpolation property (6.53) we obtain a posteriori error estimate for the regularized solution :

$$\|E - E_\tau\|_{L_2(\Omega_t)} \leq \frac{D}{\gamma} \|E - E_\tau^I\|_{L_2(\Omega_t)} \leq \frac{D}{\gamma} C_I \|\tau E\|_{H^1(\Omega_t)}. \quad (6.62)$$

We can estimate the term $\|\tau E\|_{H^1(\Omega_t)}$ in the right hand side of (6.62) similarly as in (6.54). Substituting the estimate (6.54) into the right hand side of (6.62) we get

$$\|E - E_\tau\|_{L_2(\Omega_t)} \leq \frac{D}{\gamma} C_I \left(\|\tau E_\tau\|_{L_2(\Omega_t)} + \sum_{J_k} \| [E_\tau] \|_{L_2(J_k)} \right) \quad \forall E_\tau \in V_\tau^E.$$

□

Theorem 3

Let $E_\tau \in V_\tau^E$ be a finite element approximation of the minimizer $E \in L^2(\Omega_t)$ on the finite element mesh J_τ . Then there exists an interpolation constant C_I independent on the mesh function τ such that the following a posteriori error estimate holds for $\gamma > 0$:

$$\|E - E_\tau\|_{L_2(\Omega_t)} \leq \frac{\|R(E_\tau)\|_{L_2(\Omega_t)}}{\gamma} \quad \forall E_\tau \in V_\tau^E, \quad (6.63)$$

where $R(E_\tau)$ is the residual defined as

$$R(E_\tau) = \gamma(E_\tau - E^0) + d\lambda_{2\tau} u_{2\tau}. \quad (6.64)$$

Proof.

Let again E_τ be the minimizer of the Tikhonov functional (4.9). Strong convexity of the functional (4.9) on the space $L_2(\Omega_t)$ implies that

$$\gamma \|E - E_\tau\|_{L_2(\Omega_t)}^2 \leq \| (J'(E) - J'(E_\tau), E - E_\tau) \|_{L_2(\Omega_t)}. \quad (6.65)$$

Applying splitting (6.49) to (6.65) we obtain (6.60) where the term $J'(E_\tau)$ can be written via (4.23). More precisely, when $u(t), \lambda(t)$ are exact solutions of the forward and adjoint problems, respectively, we have for E_τ :

$$L(v(E_\tau)) = J(E_\tau),$$

and thus, one can write

$$J'(E_\tau) = L'(E_\tau) = \gamma(E_\tau - E^0) + d\lambda_{2\tau} u_{2\tau}. \quad (6.66)$$

We can write estimate (6.65) as

$$\gamma \|E - E_\tau\|_{L_2(\Omega_t)} \leq \|J'(E) - J'(E_\tau)\|_{L_2(\Omega_t)}$$

Then noting that $J'(E) = 0$ and using (6.66) for approximations $u_{2\tau}, \lambda_{2\tau}$ of u_2, λ_2 , respectively, we get

$$\|E - E_\tau\|_{L_2(\Omega_t)} \leq \frac{\|R(E_\tau)\|_{L_2(\Omega_t)}}{\gamma} \quad (6.67)$$

where $R(E_\tau)$ is the residual defined as in (6.64).

□

Algorithm 1 Conjugate Gradient Algorithm (CGA)

- 1: Choose time partition J_τ of the time interval $(0, T)$. Choose initial value of the regularization parameter γ_0 , step size β_0 and the initial approximation E_τ^0 . Compute approximations of E_τ^m , $m = 1, \dots, M$ in the following steps.
- 2: Use the Newton's method on the time partition J_τ to compute approximate solutions $u_\tau^m = u_\tau(E_\tau^m, t), \lambda_\tau^m = \lambda_\tau(E_\tau^m, t)$ of the state (2.3) and adjoint (4.18) problems via iterative schemes (5.33), (5.40), respectively.
- 3: Compute gradient $G^m(t_i)$ by (7.70).
- 4: Update the unknown parameter $E := E_\tau^{m+1}$ as

$$E_\tau^{m+1}(t_i) = E_\tau^m(t_i) + r^m d^m(t_i)$$

with

$$d^m(t_i) = -G^m(t_i) + \beta^m d^{m-1}(t_i),$$

and

$$r^m = -\frac{(G^m, d^m)}{\gamma_m \|d^m\|^2}, \quad (6.68)$$

$$\beta^m = \frac{\|G^m(t_i)\|^2}{\|G^{m-1}(t_i)\|^2},$$

where $d^0(t_i) = -G^0(t_i)$ and $G^m(t_i)$ is the gradient vector which is computed by (7.70) in time moments t_i .

- 5: Update the regularization parameter γ_m for any $p \in (0, 1)$ via iterative rule of [7]

$$\gamma_m = \frac{\gamma_0}{(m+1)^p} \quad (6.69)$$

- 6: Choose the tolerance $0 < \theta < 1$ and stop computing the functions E_τ^m if either $\|G^m\|_{L_2(\Omega_t)} \leq \theta$, or norm of the computed gradient $\|G^m\|_{L_2(\Omega_t)}$ abruptly grow, or relative norms of the computed parameter $\frac{\|E_\tau^m - E_\tau^{m-1}\|}{\|E_\tau^m\|}$ are stabilized. Otherwise, set $m := m + 1$ and go to Step 2.
-

7 Optimization algorithms

This sections presents two different optimization algorithms for solution of PIP: conjugate gradient algorithm (CGA) and time-adaptive conjugate gradient algorithm (ACGA). The CGA algorithm is a standard one and can be used on a mesh with the equidistant time step τ_k on every time interval J_k . The ACGA is used for minimization of the functional (4.9) on a locally adaptively refined meshes in time and thus, the computational mesh may have different mesh sizes τ_k on every time interval J_k - see definition of partition J_τ in section 5.

Let us denote the nodal value of the gradient at every iteration m of the CGA at the observation

points $\{t_i\}$ by $G^m(t_i)$ and compute it accordingly to (4.23) as

$$G^m(t_i) = \gamma(E_\tau^m(t_i) - E_\tau^0(t_i)) + d(t_i) \lambda_{3\tau}^m(t_i) u_{2\tau}^m(t_i). \quad (7.70)$$

The approximations of solutions $u_{2\tau}^m$ and $\lambda_{3\tau}^m$ in the expression for gradient (7.70) are obtained via solution of the forward and adjoint problems, respectively, via Newton's method taking $E := E_\tau^m$. Algorithm 1 describes explicitly all steps of CGA algorithm.

In the formulation of an adaptive algorithm ACGA we have used Theorem 3 for the estimation of the error $e^k = \|E_\tau^{M,k} - E\|_{L_2(\Omega_t)}$ computed on the locally k times refined meshes J_τ^k . We choose the tolerance $0 < \theta < 1$ and run ACGA algorithm until

$$e^k = \|E_\tau^{M,k} - E\|_{L_2(\Omega_t)} \leq \theta,$$

where e^k is estimated via a posteriori error estimate (6.63) of the Theorem 3. Here, $E_\tau^{M,k}$ is the computed parameter obtained at the final iteration M of the CGA algorithm on k times refined mesh J_τ^k . For the time-mesh refinements we use the following criterion.

Algorithm 2 Adaptive Conjugate Gradient Algorithm (ACGA)

- 1: Choose initial time partition J_τ^0 of the time interval $(0, T)$. Choose initial value of the regularization parameter γ_0^0 , step size in CGA β_0^0 , and the initial approximation $E_\tau^{0,0}$. Initialize data $g_1^0 := g_1, g_2^0 = g_2$. For mesh refinements $k = 0, \dots, N$ perform following steps:
- 2: Compute $E_\tau^{M,k}$ on the time mesh J_τ^k using steps 2-6 in CGA algorithm. Here, $E_\tau^{M,k}$ is the computed parameter obtained in the CGA algorithm at the final iteration M on the k times refined mesh J_τ^k .
- 3: Refine the time mesh J_τ^k at all points where

$$\frac{|R(E_\tau^{M,k})(t)|}{\gamma} \geq \tilde{\beta}_k \max_{\Omega_t} \frac{|R(E_\tau^{M,k})(t)|}{\gamma}. \quad (7.71)$$

Here, $\tilde{\beta}_k \in (0, 1)$ is the mesh refinement parameter chosen by the user.

- 4: Construct a new time partition J_τ^{k+1} of the time interval $(0, T)$.
 - 5: Interpolate (alternative is chosen by the user):
 - or the initial approximation $E_\tau^{0,k}$ from the previous time partition J_τ^k to the new time partition J_τ^{k+1} .
 - or computed $E_\tau^{M,k}$ from the previous time partition J_τ^k to the new time partition J_τ^{k+1} .
 - 6: Interpolate data g_1^k, g_2^k from the previous time partition J_τ^k to the new time partition J_τ^{k+1} .
 - 7: Stop computations if norms of the gradients $\|G(E_\tau^{M,k})\|_{L_2(\Omega_t)}$ either increase or stabilize, compared with the previous time partition. Otherwise set $k = k + 1$ and go to Step 2.
-

The Refinements Criterion

Refine the time-mesh J_τ in neighborhoods of those time-mesh points $t \in \Omega_t$ where the weighted residual $|R(E_\tau)(t)|$ defined in (6.64) attains its maximal values:

$$\frac{|R(E_\tau)(t)|}{\gamma} \geq \tilde{\beta} \max_{\Omega_t} \frac{|R(E_\tau)(t)|}{\gamma}.$$

Here, $\tilde{\beta} \in (0, 1)$ is the tolerance number chosen by user. See discussion in [1] how this number can be chosen in optimal way. Algorithm 2 uses the above mesh refinement recommendation and implements ACGA algorithm.

8 Numerical studies

This section presents several numerical results which demonstrate performance of the time-adaptive reconstruction of the immune response function $E(t)$ in PIP using ACGA algorithm. Numerical tests are performed in Matlab R2023b. The code is available for download at [40].

In all computations we have used clinical data for the virus population function $u_3(t) \approx g_2(t)$ and for the total number of uninfected and infected T-cells $u_1(t) + u_2(t) \approx g_1(t)$ for four patients presented in the Table 3. The initial time-mesh J_τ^0 of the observation interval $[0, T] = [0, 363]$ is generated such that the time step is $\tau = 1$. We note that only data at 8 points are given in the Table 3. Since we are running CGA algorithm on the mesh J_τ^0 consisting of 364 points we first use linear interpolation to interpolate data given in the Table 3 to the data on the time mesh J_τ^0 . Next, we use interpolated data in all numerical tests for solution of PIP.

The value of the mesh refinement parameter $\tilde{\beta}_k$ in ACGA is chosen such that it allows local refinements of the time-mesh J_τ^k where k is number of mesh refinements. All computations presented below are performed for the mesh refinement parameter $\tilde{\beta}_k = 0.875$ in (7.71) for all mesh refinements k .

We compute also relative residuals R_1, R_2 between computed functions $u_{3\tau}^{M,k}, u_{1\tau}^{M,k} + u_{2\tau}^{M,k}$ and interpolated measured $V_\tau^k = g_{2\tau}^k, \Sigma_\tau^k = g_{1\tau}^k$ which are defined as

$$R_1 = \frac{|\log_{10} u_{3\tau}^{M,k} - \log_{10} g_{2\tau}^{M,k}|}{\text{nno}},$$

$$R_2 = \frac{|\log_{10}(u_{1\tau}^{M,k} + u_{2\tau}^{M,k}) - \log_{10} g_{1\tau}^k|}{\text{nno}} \quad (8.72)$$

In all computations we choose parameters in the model system (2.4) as in the Table 1. The initial data is defined as follows:

$$\begin{aligned} u_1(0) &= 1125000; \\ u_2(0) &= 0; \\ u_3(0) &= 1. \end{aligned} \quad (8.73)$$

Since CGA and ACGA algorithms are locally convergent it is of vital importance that the initial guess $E^0(t)$ for approximation of the function $E(t)$ satisfy conditions (2.6) what means that E^0 is located in the close neighborhood of the exact function $E(t)$. We model the initial guess $E^0(t)$ for

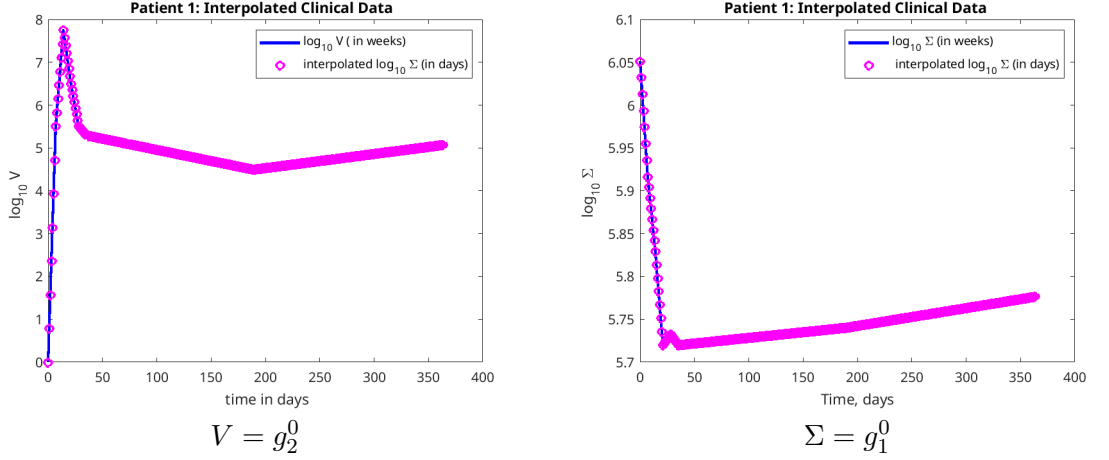


Figure 3: Patient 1: Interpolated clinical data by linear spline.

the function $E(t)$ with inclusion of such called cytotoxic T lymphocyte (CTL) response in $E^0(t)$, as it was proposed in [30].

In all our tests we have modelled effect of the CTL response for both functions $d(t)$, $E^0(t)$ as follows:

$$\begin{aligned}
d(t) &= d_0 + d_1(t, V), \\
d_1(t, u_3) &= \begin{cases} 0, t < t_1, \\ f(t) \log_{10} V, t \geq t_1, \end{cases} \\
E^0(t) &= E_0^0 + d_1(t, V), \\
f(t) &= \frac{\beta_{CTL}}{1 + \kappa e^{-(t-t_1)/\delta T_1}} - \frac{\beta_{CTL}}{1 + \kappa e^{-(t-t_2)/\delta T_2}}, \\
\kappa &= 1 + 10^5 \beta_{CTL}.
\end{aligned} \tag{8.74}$$

Parameter values for all parameters in (8.74) are chosen differently for all patients such that they give as good as possible fitting to data. Detailed values of parameters are given in the next subsections.

8.1 Results for Patient 1

In computations of boths, CGA and ACGA, algorithms for patient 1 we used interpolated clinical data of the Table 2 presented in the Figure 3. Next, we define the initial guess for the immune response function E_0 in optimization algorithms using (8.74). For patient 1 the parameters in (8.74)

are chosen as follows:

$$\begin{aligned}
d_0 &= 0.26; \\
\beta_{CTL} &= 0.015; \\
\kappa &= 1 + 10^5 \beta_{CTL}; \\
\delta T_1 &= 2.5; \\
\delta T_2 &= 5.0; \\
E_0^0 &= 1, \\
t_1 &= 1, \\
t_2 &= 1.
\end{aligned} \tag{8.75}$$

Figures 4 show time-dependent functions for initial guess $E^0(t)$ as well as $f(t), d(t)$ with CTL response for parameters defined in (8.75). These functions are used now in optimization algorithms for reconstruction of the immune response function $E(t)$. Figures 5 show computed functions E_τ^k on k times adaptively refined meshes J_τ^k in ACGA algorithm.

Figures 6 show time-dependent behaviour of the computed virus function $V_\tau^k, k = 0, 4$ before and after applying ACGA. Here, the computed virus function V_τ^k corresponds to the computed E_τ^k presented in Figure 5. Results are compared with clinical data for the observed virus function $V = g_2^0$ and observed total number of the uninfected and infected cells $\Sigma = g_1^0$. Figure 6-b) shows computed virus function on the four times locally refined time mesh J_τ^4 . Computed optimized virus function on $J_\tau^k, k = 0, 1, 2, 3$ has similar behaviour and is not presented here.

Figures 7 show stabilization of the computed relative norms $\frac{\|E_\tau^m - E_\tau^{m-1}\|_{L_2(\Omega_t)}}{\|E_\tau^m\|_{L_2(\Omega_t)}}$ and behaviour of norms of the computed gradient $\|G^m(t)\|_{L_2(\Omega_t)}$ for patient 1. Relative residuals R_1 and R_2 and $\|R_1\|_{L_2(\Omega_t)}, \|R_2\|_{L_2(\Omega_t)}$ which are computed as in (8.72) on the locally refined meshes J_τ^k are presented in the Table 4 as well as in the Figures 8. All these norms are used in ACGA in the stopping criterion.

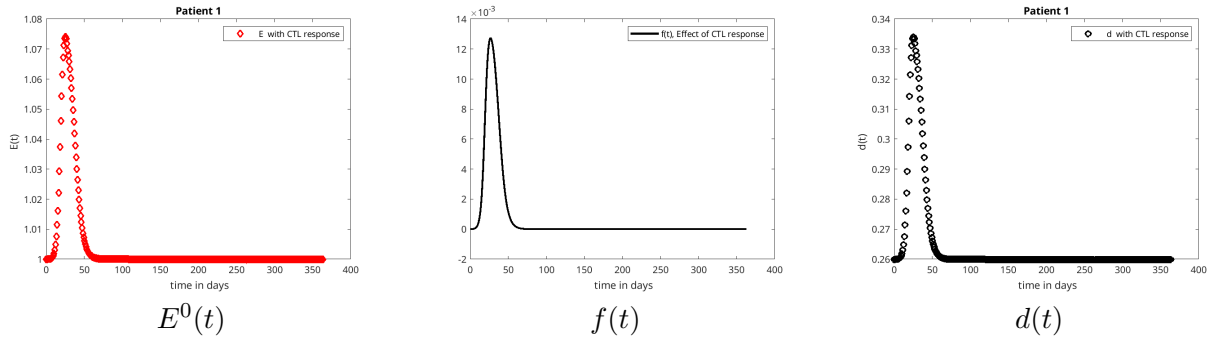


Figure 4: Patient 1: functions $E^0(t)$, $f(t)$, $d(t)$ with CTL response modelled as in (8.74) using parameters defined in (8.75).

k	nno	$\ R_1\ $	$\ R_2\ $
0	364	0.0880	0.0382
1	516	0.0769	0.0321
2	518	0.0767	0.0320
3	522	0.0762	0.0320
4	530	0.0753	0.0320

a) Patient 1			
k	nno	$\ R_1\ $	$\ R_2\ $
0	364	0.1321	0.0412
1	410	0.1215	0.0389

b) Patient 2			
k	nno	$\ R_1\ $	$\ R_2\ $
0	364	0.1802	0.0407
1	413	0.165	0.0384
2	478	0.1464	0.0358

c) Patient 3			
k	nno	$\ R_1\ $	$\ R_2\ $
0	364	0.1643	0.0434
1	385	0.1560	0.0421
2	402	0.1495	0.0411

d) Patient 4			
k	nno	$\ R_1\ $	$\ R_2\ $
0	364	0.1802	0.0407
1	413	0.165	0.0384
2	478	0.1464	0.0358

Table 4: Computed norms of the residuals R_1 and R_2 defined by (8.72) on the meshes J_τ^k . Here, nno is the number of nodes in the time-mesh.

8.2 Results for Patient 2

For patient 2 we used interpolated clinical data of the Table 2 presented in the Figure 9.

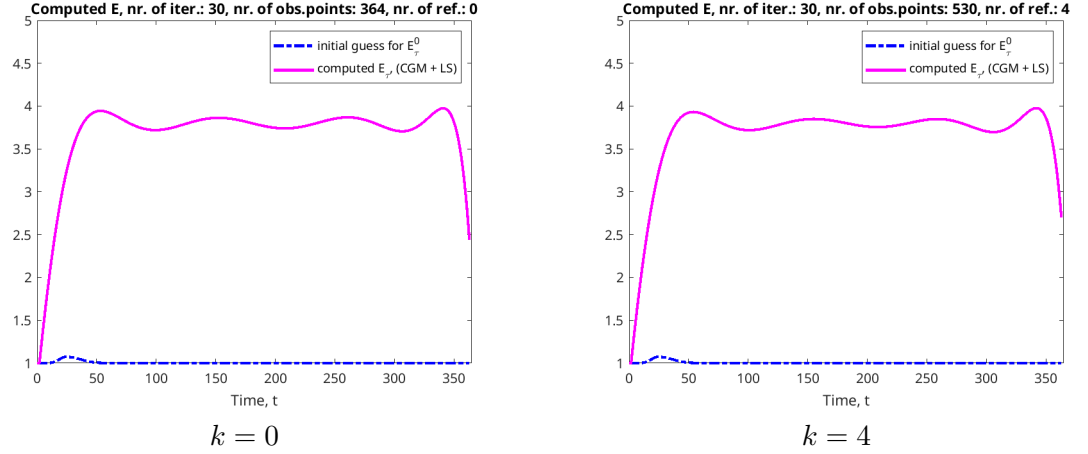


Figure 5: Patient 1: results of reconstruction of the function $E(t)$ on k times adaptively refined meshes J_τ^k in ACGA algorithm. Computations are performed for the mesh refinement parameter $\tilde{\beta}_k = 0.875$ for all mesh refinements k .

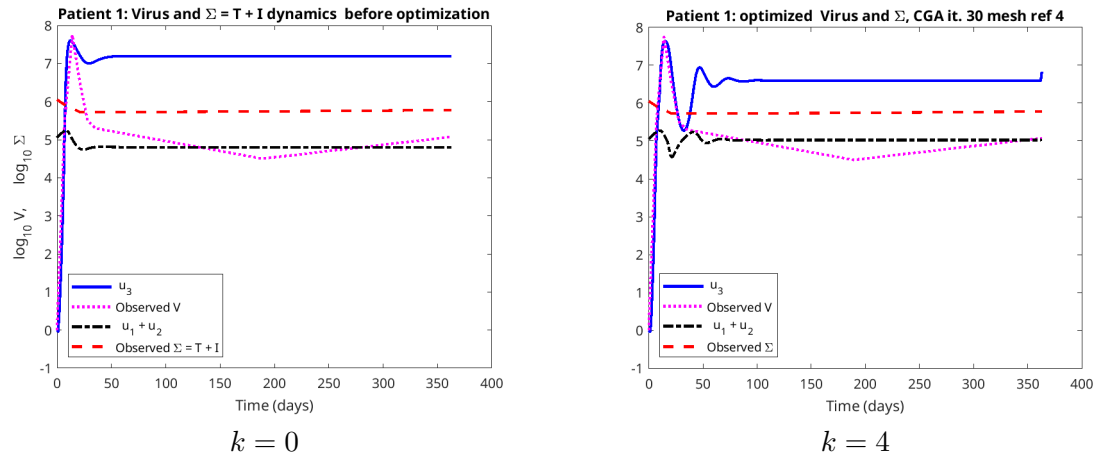


Figure 6: Patient 1: Dynamics of the computed virus function V_τ^k before and after optimization corresponding to the computed E_τ^k on k times adaptively refined meshes versus interpolated clinical data $g_{1\tau}^0, g_{2\tau}^0$.

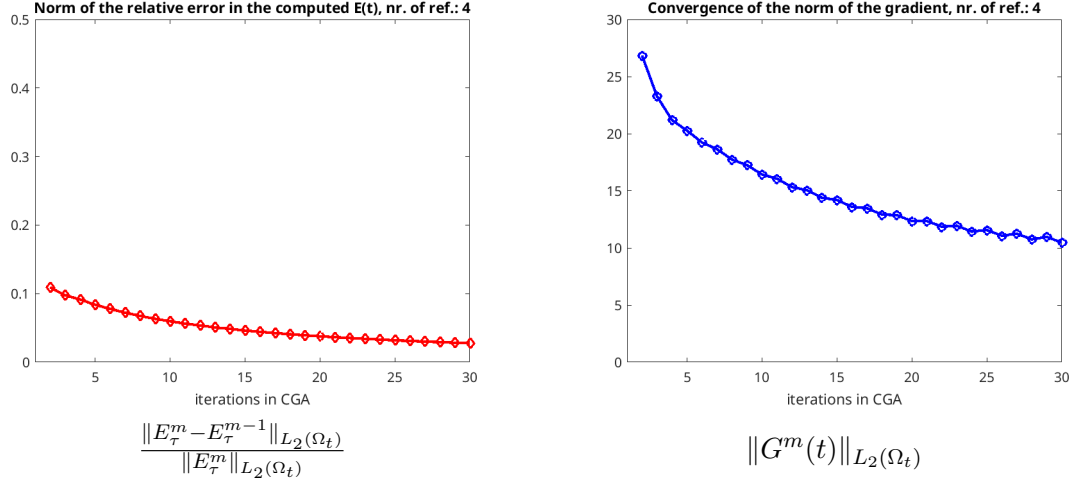


Figure 7: Patient 1: computed relative norms $\frac{\|E_\tau^m - E_\tau^{m-1}\|_{L_2(\Omega_t)}}{\|E_\tau^m\|_{L_2(\Omega_t)}}$ and $\|G^m(t)\|_{L_2(\Omega_t)}$ on the mesh J_τ^4 .

For patient 2 we define the parameters in (8.74) as follows:

$$\begin{aligned}
 d_0 &= d = 0.26; \\
 \beta_{CTL} &= 0.1; \\
 \kappa &= 1 + 10^5 \beta_{CTL}; \\
 \delta T_1 &= 2.5; \\
 \delta T_2 &= 5.0; \\
 E_0^0 &= 1, \\
 t_1 &= 1, \\
 t_2 &= 50.
 \end{aligned} \tag{8.76}$$

Figures 10 show time-dependent functions for initial guess $E^0(t)$ as well as $f(t), d(t)$ with CTL response for parameters defined in (8.75). These functions are used now in optimization algorithms for reconstruction of the immune response function $E(t)$. Figures 11 show computed functions E_τ^k on $k = 0, 1$ times adaptively refined meshes J_τ^k .

Figures 12 show time-dependent behaviour of the computed virus function $V_\tau^k, k = 0, 1$ before and after applying ACGA. Here, the computed virus function V_τ^k corresponds to the computed E_τ^k presented in Figure 11. Results are compared with clinical data for the observed virus function $V = g_2^0$ and observed total number of the uninfected and infected cells $\Sigma = g_1^0$. Computed optimized virus function on J_τ^0 is presented in the Figure 12-b). Figure 12-c) shows computed virus function on the one time locally refined time mesh J_τ^1 . Comparing figures 12-b) and 12-c) we observe that local adaptive mesh refinement allows more exact fit data to achieve minimum of the virus load. Figures 13 show stabilization of the computed relative norms $\frac{\|E_\tau^m - E_\tau^{m-1}\|_{L_2(\Omega_t)}}{\|E_\tau^m\|_{L_2(\Omega_t)}}$ and behaviour of

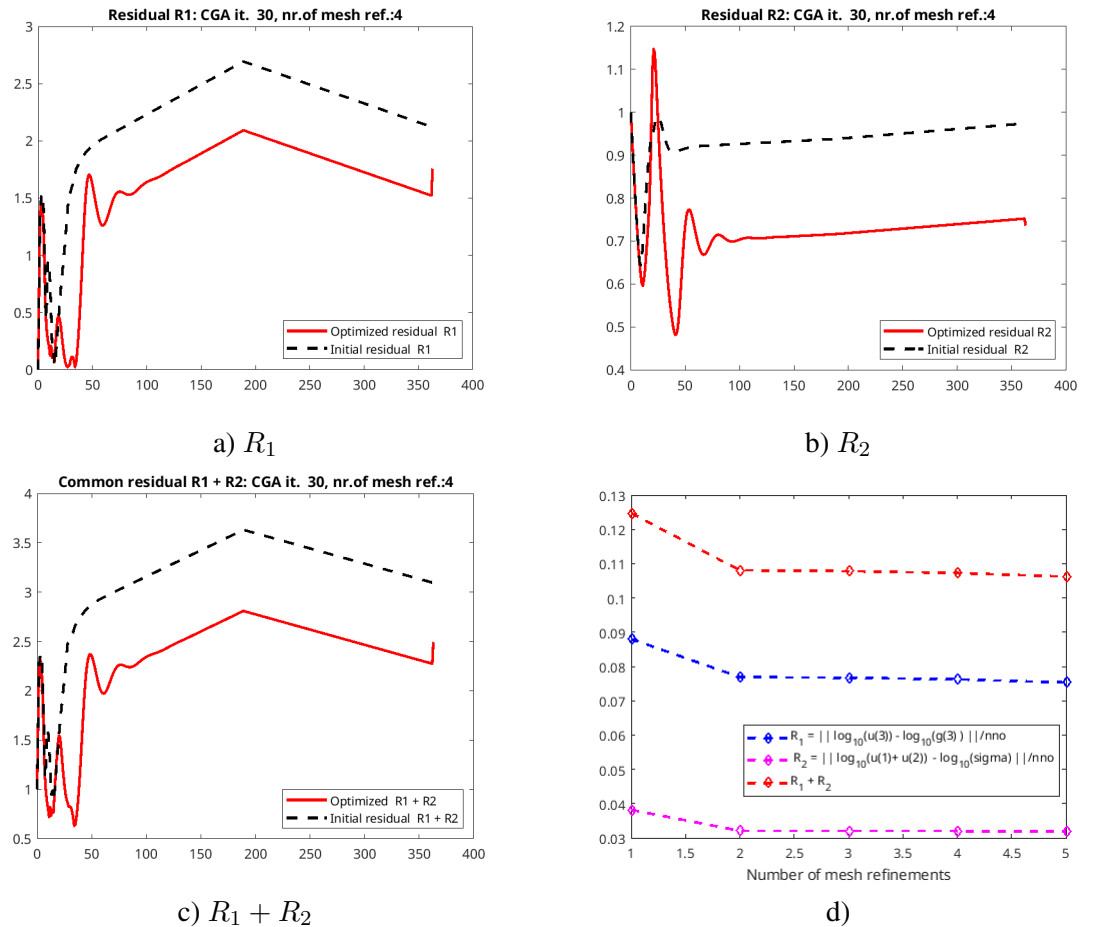


Figure 8: Patient 1: a), b), c) computed residuals R_1 and R_2 on the mesh J_t^4 ; d) Comparison of related residuals $\|R_1\|$, $\|R_2\|$ on different refined meshes J_t^k , $k = 0, \dots, 4$.

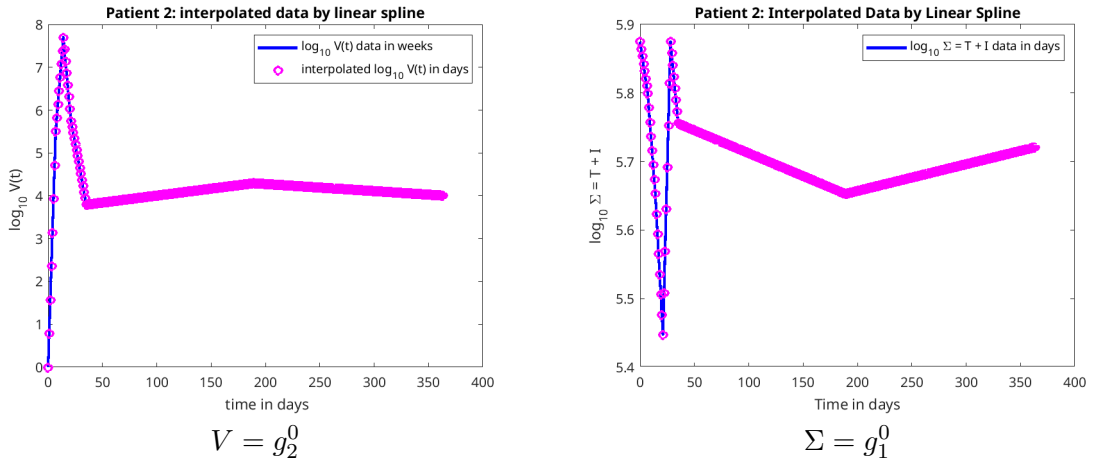


Figure 9: Patient 2: Interpolated clinical data by linear spline.

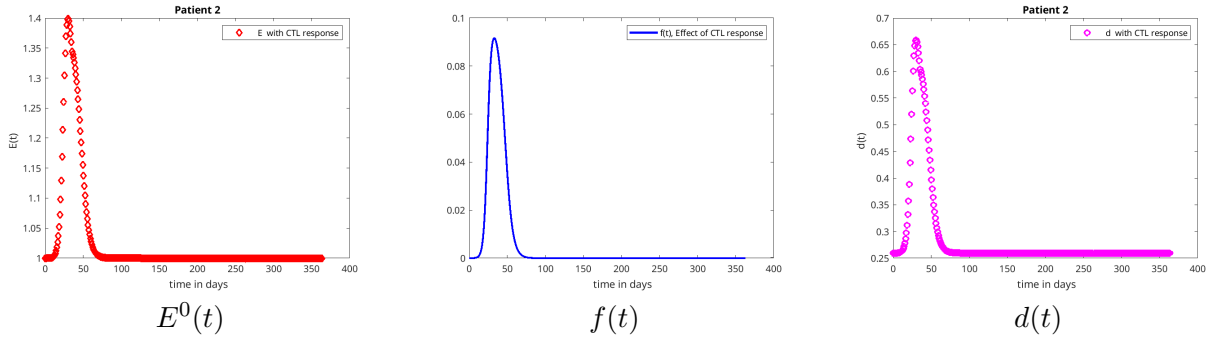


Figure 10: Patient 2: functions $E^0(t)$, $f(t)$, $d(t)$ with CTL response modelled as in (8.74) using parameters defined in (8.75).

norms of the computed gradient $\|G^m(t)\|_{L_2(\Omega_t)}$ for patient 2. Relative residuals R_1 and R_2 and $\|R_1\|_{L_2(\Omega_t)}$, $\|R_2\|_{L_2(\Omega_t)}$ are presented in the Figures 14 as well as in the Table 4.

8.3 Results for Patient 3

For patient 3 we used interpolated clinical data of the Table 2 presented in the Figure 15. We set all parameters in (8.74) the same as for patient 2.

Figures 10 show time-dependent functions for initial guess $E^0(t)$ as well as $f(t)$, $d(t)$ with CTL

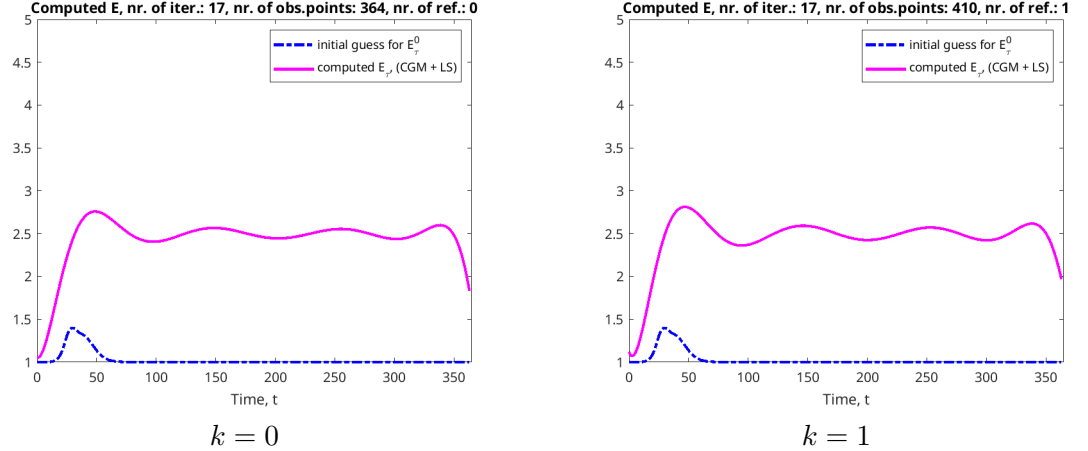


Figure 11: Patient 2: results of reconstruction of the function $E(t)$ on k times adaptively refined meshes J_τ^k in ACGA algorithm. Computations are performed for the mesh refinement parameter $\tilde{\beta}_k = 0.875$ for all mesh refinements k .

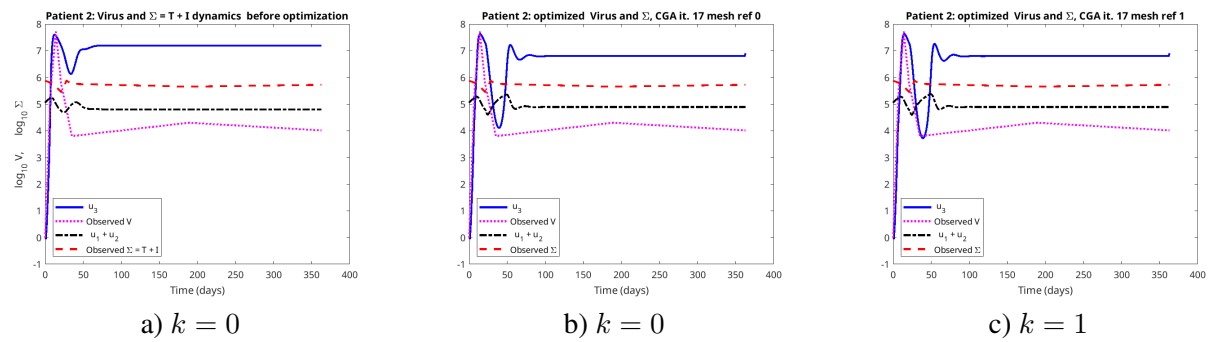


Figure 12: Patient 2: Dynamics of the computed virus function V_τ^k before and after optimization corresponding to the computed E_τ^k on $k, k = 0, 1$ times adaptively refined meshes versus interpolated clinical data $g_{1\tau}^0, g_{2\tau}^0$.

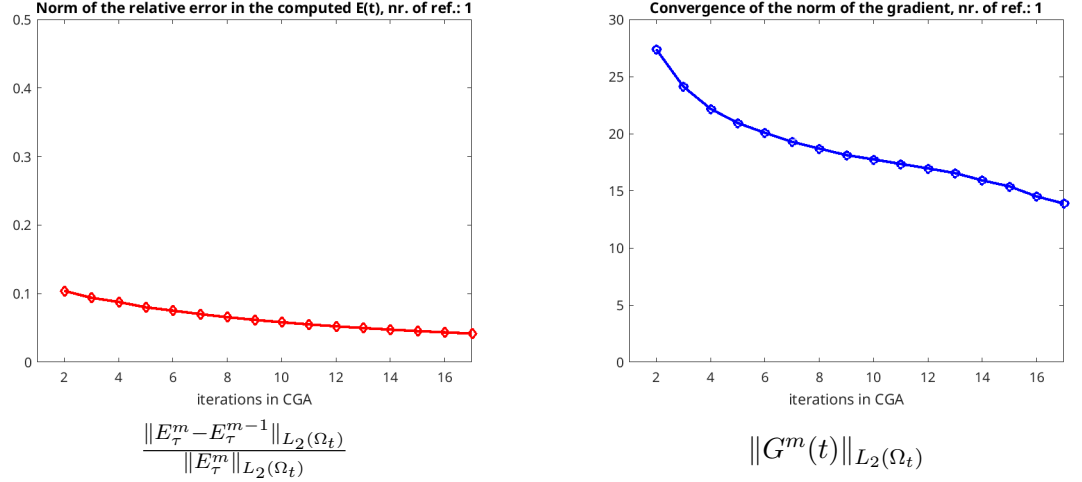


Figure 13: Patient 2: computed relative norms $\frac{\|E_\tau^m - E_\tau^{m-1}\|_{L_2(\Omega_t)}}{\|E_\tau^m\|_{L_2(\Omega_t)}}$ and $\|G^m(t)\|_{L_2(\Omega_t)}$ on the mesh J_τ^1 .

response for parameters defined in (8.75) which are the same as for the patient 2. These functions are used now in optimization algorithms for reconstruction of the immune response function $E(t)$. Figures 16 show computed functions E_τ^k on $k = 0, 1, 2$ times adaptively refined meshes J_τ^k .

Figures 17 show time-dependent behaviour of the computed virus function $V_\tau^k, k = 0, 2$ before and after applying ACGA. Here, the computed virus function V_τ^k corresponds to the computed E_τ^k presented in Figure 16. Results are compared with clinical data for the observed virus function $V = g_2^0$ and observed total number of the uninfected and infected cells $\Sigma = g_1^0$. Computed optimized virus function on J_τ^0 is presented in the Figure 17-b). Figure 17-c) shows computed virus function on the twice locally refined time mesh J_τ^2 . Comparing figures 17-b) and 17-c) we again observe that local adaptive mesh refinement allows more exact fit data to achieve minimum of the virus load. Figures 18 show stabilization of the computed relative norms $\frac{\|E_\tau^m - E_\tau^{m-1}\|_{L_2(\Omega_t)}}{\|E_\tau^m\|_{L_2(\Omega_t)}}$ and behaviour of norms of the computed gradient $\|G^m(t)\|_{L_2(\Omega_t)}$ for patient 3. Relative residuals R_1 and R_2 and $\|R_1\|_{L_2(\Omega_t)}, \|R_2\|_{L_2(\Omega_t)}$ are presented in the Figures 19 as well as in the Table 4.

8.4 Results for Patient 4

For patient 4 we used interpolated clinical data of the Table 2 presented in the Figure 20. We observe that the data is very discontinuous. However, we test the same ACGA algorithm for this dataset to see performance of the code.

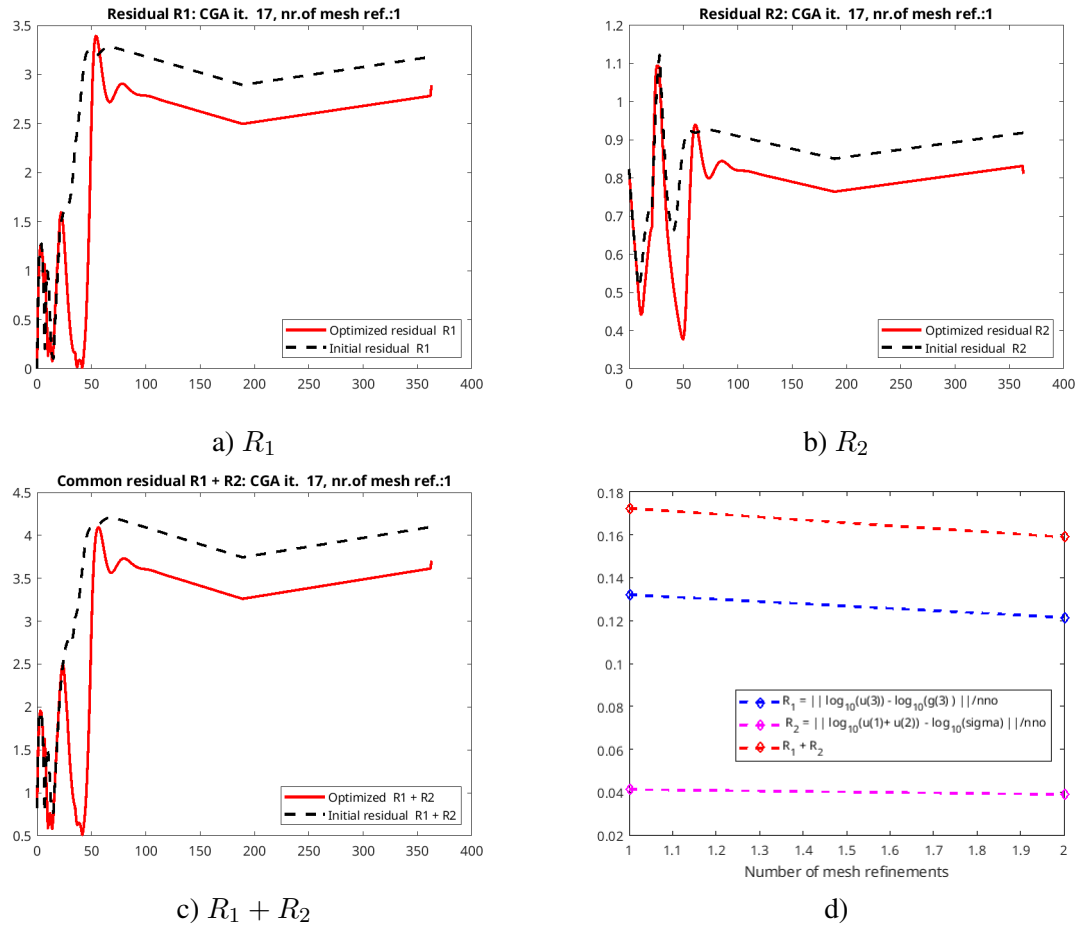


Figure 14: Patient 2: a), b), c) computed residuals R_1 and R_2 on the mesh J_τ^1 ; d) Comparison of related residuals $\|R_1\|$, $\|R_2\|$ on the meshes J_τ^k , $k = 0, 1$.

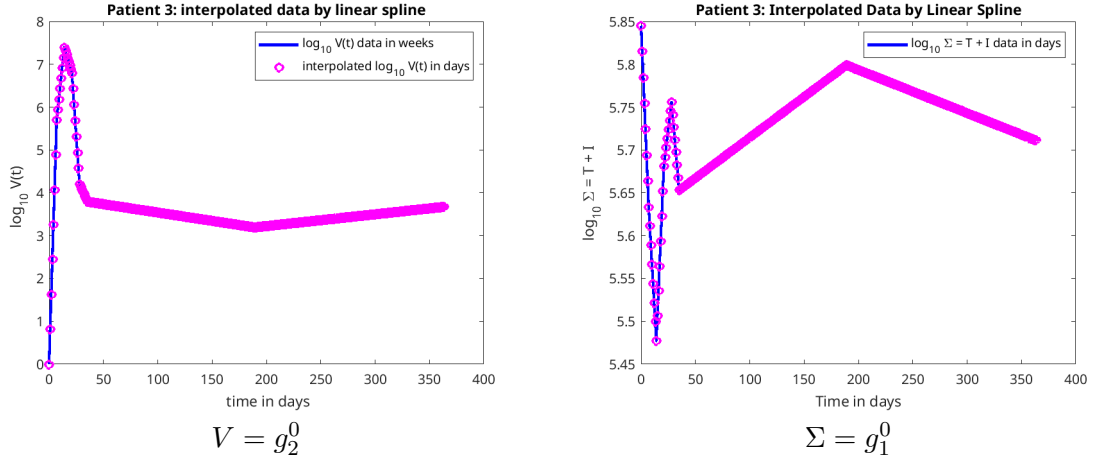


Figure 15: Patient 3: Interpolated clinical data by linear spline.

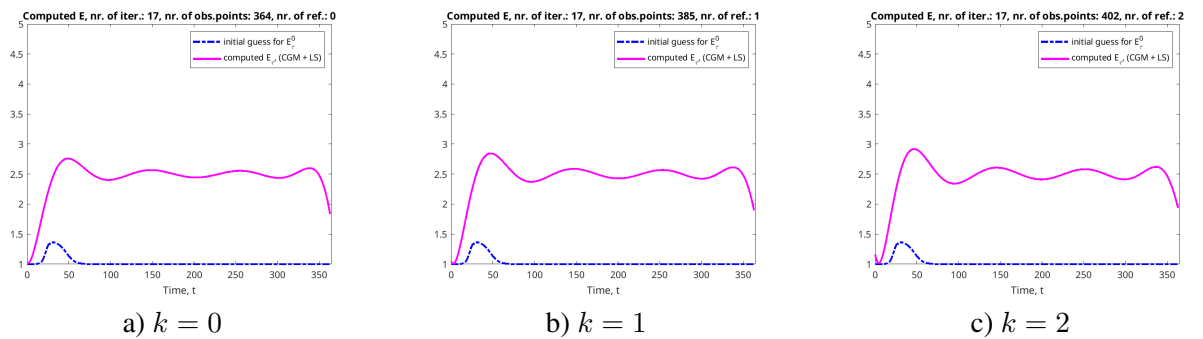


Figure 16: Patient 3: results of reconstruction of the function $E(t)$ on k times adaptively refined meshes J_τ^k in ACGA algorithm. Computations are performed for the mesh refinement parameter $\tilde{\beta}_k = 0.875$ for all mesh refinements k .

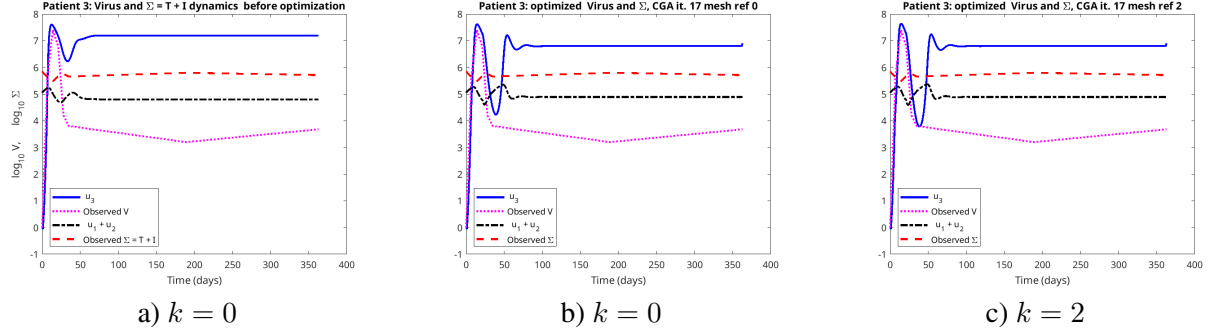


Figure 17: Patient 3: Dynamics of the computed virus function V_τ^k before and after optimization corresponding to the computed E_τ^k on $k, k = 0, 2$ times adaptively refined meshes versus interpolated clinical data $g_{1\tau}^0, g_{2\tau}^0$.

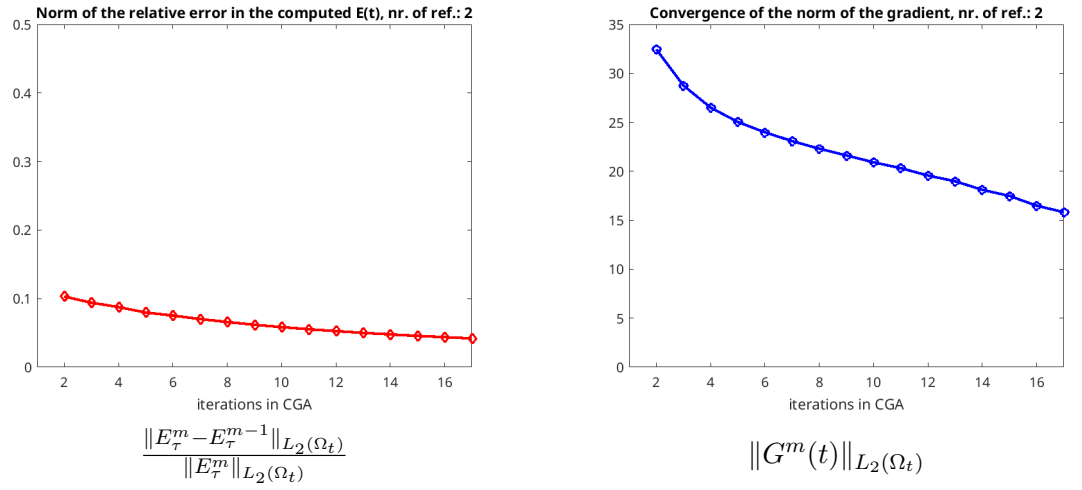


Figure 18: Patient 3: computed relative norms $\frac{\|E_\tau^m - E_\tau^{m-1}\|_{L_2(\Omega_t)}}{\|E_\tau^m\|_{L_2(\Omega_t)}}$ and $\|G^m(t)\|_{L_2(\Omega_t)}$ on the mesh J_τ^2 .

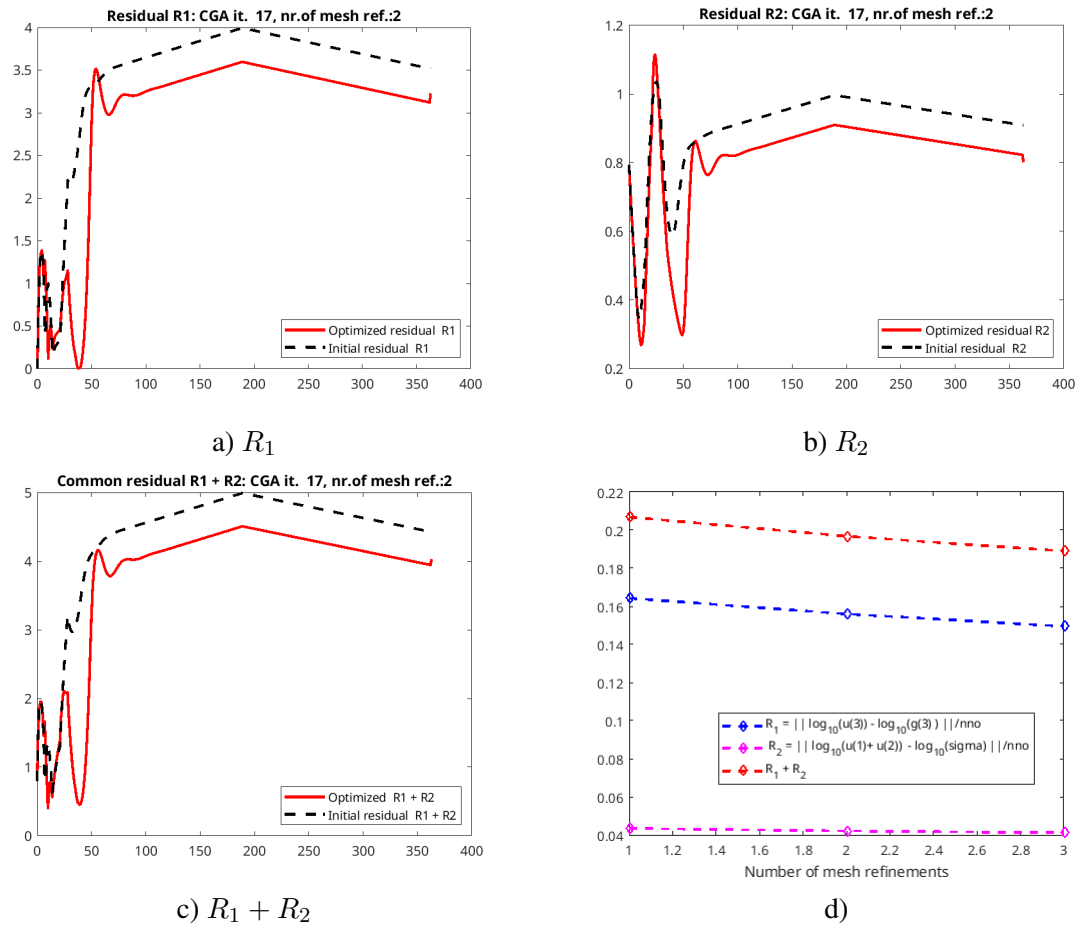


Figure 19: Patient 3: a), b), c) computed residuals R_1 and R_2 on the mesh J_τ^2 ; d) Comparison of related residuals $\|R_1\|$, $\|R_2\|$ on the meshes J_τ^k , $k = 0, 1, 2$.

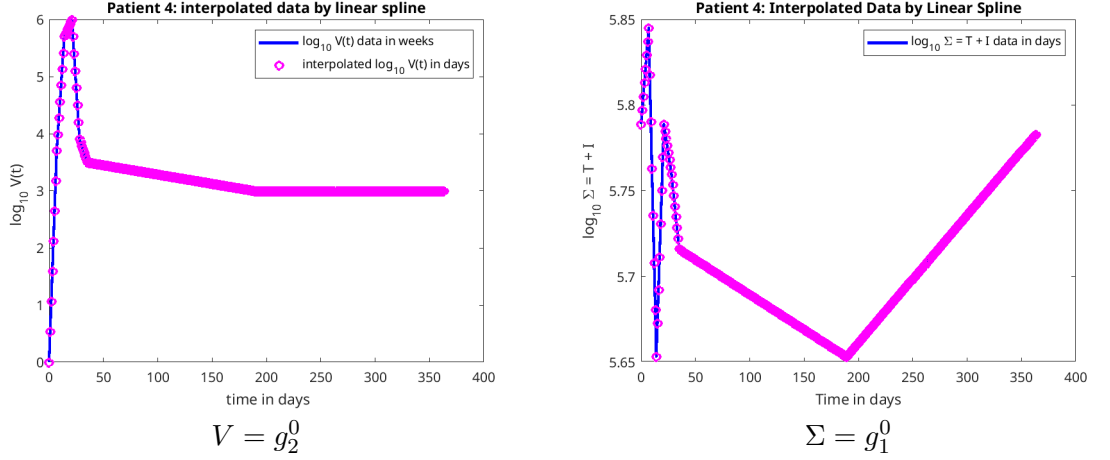


Figure 20: Patient 4: Interpolated clinical data by linear spline.

For patient 4 we define the parameters in (8.74) as follows:

$$\begin{aligned}
 d_0 &= d = 0.26; \\
 \beta_{CTL} &= 0.1; \\
 \kappa &= 1 + 10^5 \beta_{CTL}; \\
 \delta T_1 &= 2.5; \\
 \delta T_2 &= 5.0; \\
 E_0 &= 1.4, \\
 t_1 &= 1, \\
 t_2 &= 1.
 \end{aligned} \tag{8.77}$$

Figures 21 show time-dependent functions for initial guess $E^0(t)$ as well as $f(t), d(t)$ with CTL response for parameters defined in (8.75) which are the same as for the patient 4. These functions are used now in optimization algorithms for reconstruction of the immune response function $E(t)$. Figures 22 show computed functions E_τ^k on $k = 0, 1, 2$ times adaptively refined meshes J_τ^k .

Figures 23 show time-dependent behaviour of the computed virus function $V_\tau^k, k = 0, 2$ before and after applying ACGA. Here, the computed virus function V_τ^k corresponds to the computed E_τ^k presented in Figure 22. Results are compared with clinical data for the observed virus function $V = g_2^0$ and observed total number of the uninfected and infected cells $\Sigma = g_1^0$. Computed optimized virus function on J_τ^0 is presented in the Figure 23-b). Figure 23-c) shows computed virus function on the twice locally refined time mesh J_τ^2 . Comparing figures 23-b) and 23-c) we again observe that local adaptive mesh refinement allows more exact fit data to achieve minimum of the virus load. Figures 24 show stabilization of the computed relative norms $\frac{\|E_\tau^m - E_\tau^{m-1}\|_{L_2(\Omega_t)}}{\|E_\tau^m\|_{L_2(\Omega_t)}}$ and behaviour of

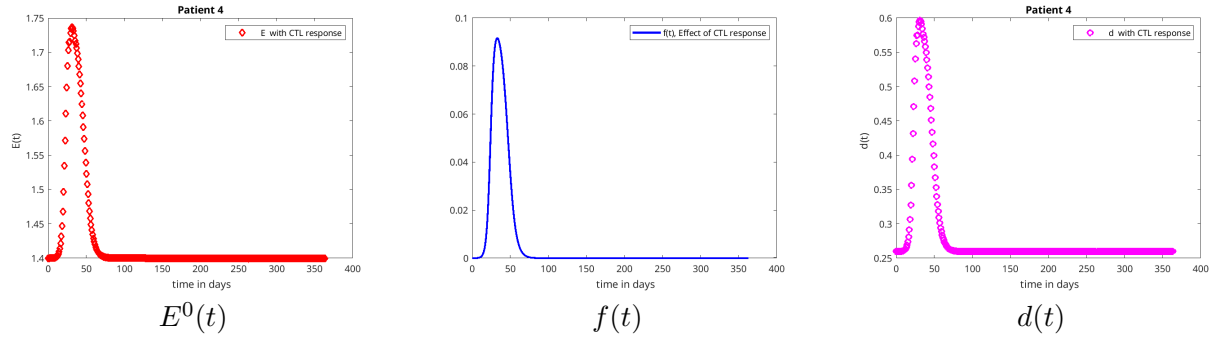


Figure 21: Patient 4: functions $E^0(t)$, $f(t)$, $d(t)$ with CTL response modelled as in (8.74) using parameters defined in (8.75).

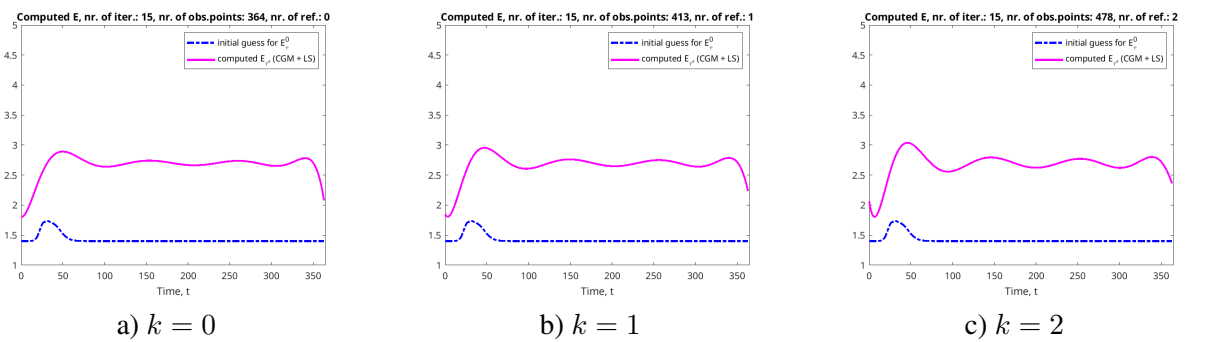


Figure 22: Patient 4: results of reconstruction of the function $E(t)$ on k times adaptively refined meshes J_r^k in ACGA algorithm. Computations are performed for the mesh refinement parameter $\tilde{\beta}_k = 0.875$ for all mesh refinements k .

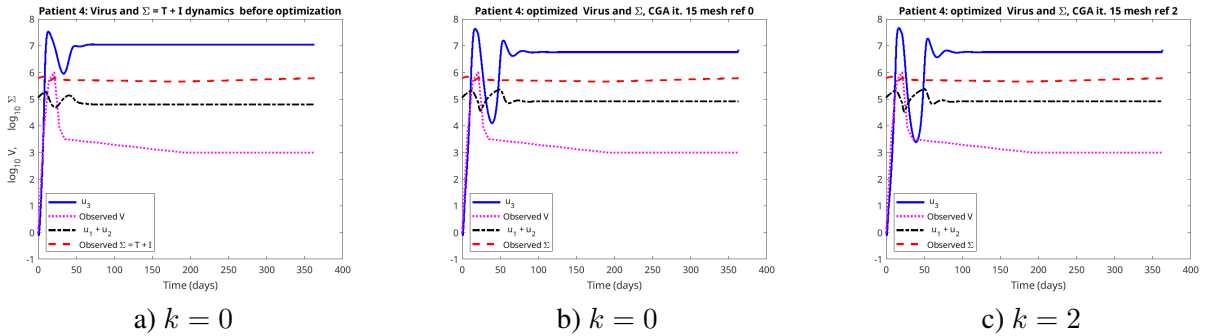


Figure 23: Patient 4: Dynamics of the computed virus function V_τ^k before and after optimization corresponding to the computed E_τ^k on $k, k = 0, 2$ times adaptively refined meshes versus interpolated clinical data $g_{1\tau}^0, g_{2\tau}^0$.

norms of the computed gradient $\|G^m(t)\|_{L_2(\Omega_t)}$ for patient 4. Relative residuals R_1 and R_2 and $\|R_1\|_{L_2(\Omega_t)}, \|R_2\|_{L_2(\Omega_t)}$ are presented in the Figures 25 as well as in the Table 4.

9 Conclusion

We propose a time-adaptive optimization framework for determining the time-dependent immune response function within a mathematical model of acute HIV infection, using clinical data from four untreated patients.

This approach begins with estimating the immune response on a coarse initial time grid, based on several known values of the observable functions. The time grid is then locally refined at points where the residual $|R(E_\tau)(t)|$ reaches its maximal values. The immune response function is subsequently recomputed on the refined time mesh, enhancing the resolution where it is most needed.

Our methodology uses Lagrangian approach, from which we derive the optimality conditions and a numerical scheme to solve the forward problem, adjoint problem, and parameter identification problem. Furthermore, we establish three distinct a posteriori error estimates and formulate an adaptive optimization algorithm tailored to this dynamic framework.

Numerical experiments demonstrate the effectiveness of the proposed adaptive method in reconstructing the immune response during the acute phase of HIV infection, using patient-specific clinical data. These results highlight that local adaptive mesh refinement yields a more precise data fit to achieve minimum of the virus function at the acute phase of HIV infection.

However, further computational investigations are required to accurately fit clinical data over the clinical latency stage of HIV, using the same dataset.

The proposed time-adaptive optimization strategy has the potential to aid clinicians by enabling individualized parameter identification in specific PIP.

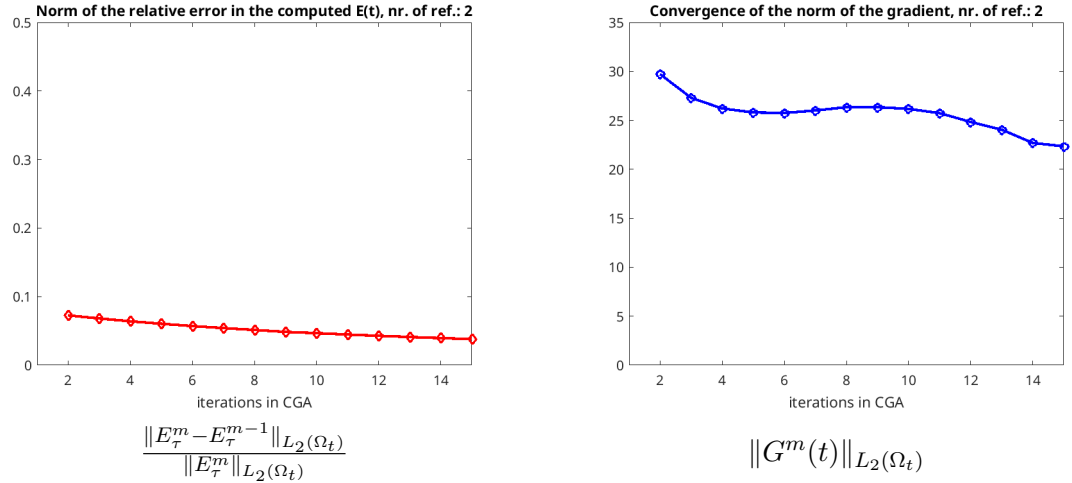


Figure 24: Patient 4: computed relative norms $\frac{\|E_\tau^m - E_\tau^{m-1}\|_{L_2(\Omega_t)}}{\|E_\tau^m\|_{L_2(\Omega_t)}}$ and $\|G^m(t)\|_{L_2(\Omega_t)}$ on the mesh J_τ^2 .

References

- [1] L. Beilina, M. Eriksson, I. Gainova, Time-adaptive determination of drug efficacy in mathematical model of HIV infection, *Differential Equations and Dynamical Systems*, 32(1), 313–347, 2024. <https://doi.org/10.1007/s12591-021-00572-w>
- [2] P. K. Srivastava, M. Banerjee, and P. Chandra, Modeling the drug therapy for HIV infection, *Journal of Biological Systems*, 17(2), 213–223, 2009.
- [3] Nowak MA, Bangham CRM, Population dynamics of immune responses to persistent viruses, *Science*, 1996. 272:74-79. <https://doi.org/10.1126/science.272.5258.74>
- [4] Nowak MA, May R, *Virus dynamics mathematical principles of immunology and virology*, Oxford University Press, Oxford, 2000.
- [5] S. W. Kazer, T. P. Aicher, D. M. Muema, et al., Integrated single-cell analysis of multicellular immune dynamics during hyperacute HIV-1 infection, *Nature Medicine*, 26:511-518, 2020.
- [6] R. J. De Boer, R. M. Ribeiro, A. S. Perelson, Current Estimates for HIV-1 Production Imply Rapid Viral Clearance in Lymphoid Tissues, *PLoS Computational Biology*, 6(9), 2010.
- [7] A. B. Bakushinskii and M. Yu. Kokurin, *Iterative Methods for Approximate Solution of Inverse Problems*, Springer, New York, 2004.
- [8] J. Albersmeyer, Adjoint Based Algorithms and Numerical Methods for Sensitivity Generation and Optimization of Large Scale Dynamic Systems, Ph.D. thesis, Heidelberg University, 2010.

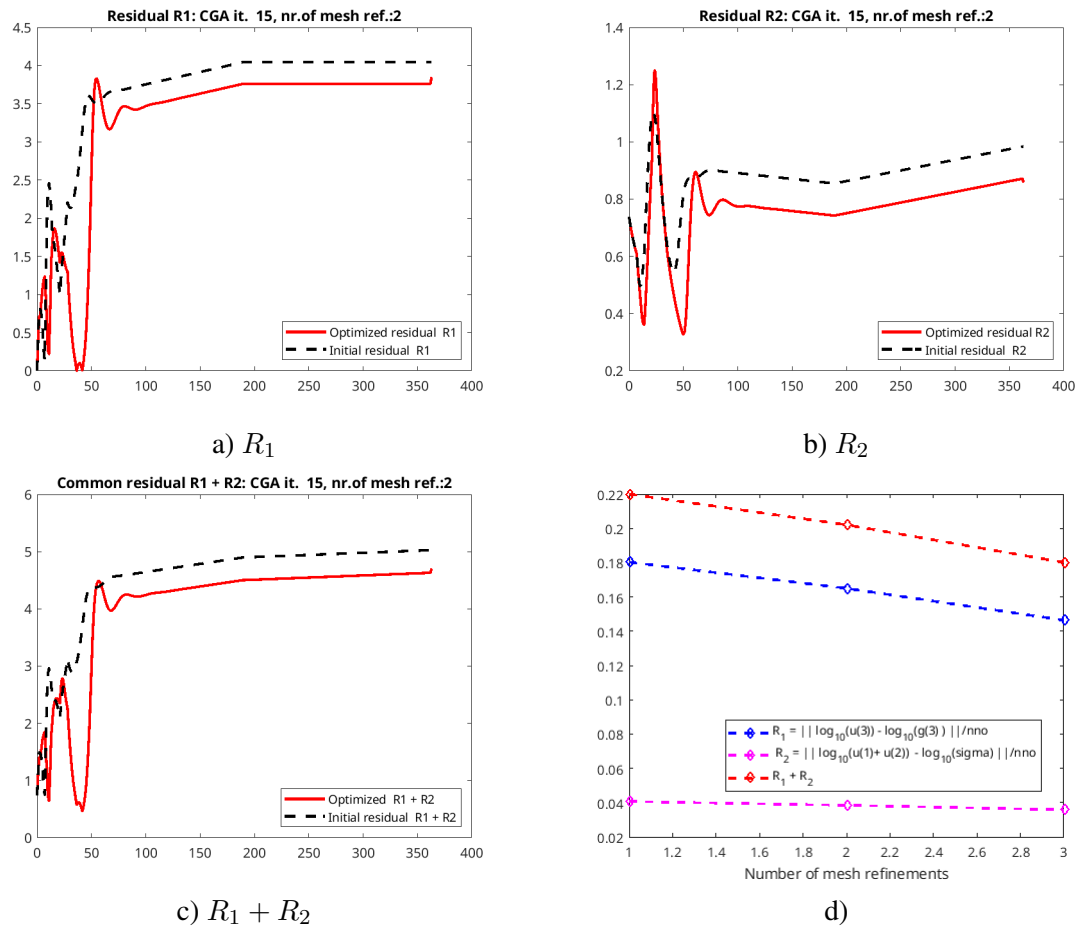


Figure 25: Patient 3: a), b), c) computed residuals R_1 and R_2 on the mesh J_τ^2 ; d) Comparison of related residuals $\|R_1\|$, $\|R_2\|$ on the meshes J_τ^k , $k = 0, 1, 2$.

- [9] E. F. Arruda, C. M. Dias, , C. V. de Magalhaes, D. H. Pastore, R. C. A. Thomé, H. M. Yang, An optimal control approach to HIV immunology, *Applied Mathematics*, 1115-1130, 2015. <http://dx.doi.org/10.4236/am.2015.66102>
- [10] A. Almudevar and E. F. Arruda, Optimal Approximation Schedules for a Class of Iterative Algorithms, With an Application to Multigrid Value Iteration, *IEEE Transactions on authomatic control*, 57(12), 2012.
- [11] H. T. Banks and K. Kunisch, *Estimation techniques for distributed parameter systems*, Birkhäuser 1989. ISBN 978-1-4612-3700-6.
- [12] L. Beilina and I. Gainova, Time-adaptive FEM for distributed parameter identification in biological models, *Applied Inverse Problems*, Springer Proceedings in Mathematics & Statistics, 48, pp.37–50, 2013.
- [13] L. Beilina and I. Gainova, Time-adaptive FEM for distributed parameter identification in mathematical model of HIV infection with drug therapy, *Inverse Problems and Applications*, Springer Proceedings in Mathematics & Statistics, 120, pp.111–124, 2015.
- [14] L. Beilina, M .V. Klibanov, *Approximate global convergence and adaptivity for Coefficient Inverse Problems*, Springer, New York, 2012.
- [15] G. Bocharov, V. Chereshnev, I. Gainova, S. Bazhan, B. Bachmetyev, J. Argilaguet, J. Martinez and A. Meyerhans, Human Immunodeficiency Virus Infection: from Biological Observations to Mechanistic Mathematical Modelling, *Mathematical Modelling of Natural Phenomena*, 7(5), 78–104, 2012.
- [16] G. Bocharov, V. Volpert, B. Ludewig, A. Meyerhans, *Mathematical Immunology of Virus Infections*, Springer/Nature 2018. ISBN 978-3-319-72317-4.
- [17] Richard L. Burden, J. Douglas Fairés, Numerical Analysis, 9th Edition, Brooks/Cole
- [18] V. A. Chereshnev, G. A. Bocharov, S. I. Bazhan, B. Bachmetyev, I. A. Gainova, V. A. Likhoshvai, J. M. Argilaguet, J. .P. Martinez, J. A.Rump, B. Mothe, C. Brander and A. Meyerhans, Pathogenesis and Treatment of HIV Infection: The Cellular, the Immune System and the Neuroendocrine Systems Perspective, *International Reviews of Immunology*, 32(3), 282–306, 2013. <http://informahealthcare.com/doi/abs/10.3109/08830185.2013.779375>
- [19] V. A. Chereshnev, G. A. Bocharov, A. V. Kim, S. I. Bazhan, I. A. Gainova, A. N. Krasovskii, N. G. Shmagel, A. V. Ivanov, M. A. Safronov, R. M. Tretyakova, *Introduction to modeling and control of HIV infection dynamics*, Institute for Computer Research, Moscow – Izhevsk, 2016. (book, in Russian)
- [20] R. Eftimie, J. J. Gillard, D. Cantrell, Mathematical Models for Immunology: Current State of the Art and Future Research Directions, *Bull.Math.Biol.*, 78(10), 2091-2134, 2016.

- [21] K. Eriksson, D. Estep and C. Johnson, *Calculus in Several Dimensions*, Springer, Berlin, 2004.
- [22] K. Hatz, J. P. Schlöder, and H. G. Bock, Estimating Parameters in Optimal Control Problems, *SIAM J. Sci. Comput.*, 34(3), 2012. <https://doi.org/10.1137/110823390>
- [23] N. Koshev and L. Beilina, An adaptive finite element method for Fredholm integral equations of the first kind and its verification on experimental data, *CEJM*, 11(8), 1489–1509, 2013.
- [24] L. M. Mansky, H. M. Temin, Lower in vivo mutation rate of human immunodeficiency virus type 1 than that predicted from the fidelity of purified reverse transcriptase, *J. Virology*, 69, 5087-5094, 1995.
- [25] D. H. Pastore, R. C. A. Thomé, C. M. Dias, E. F. Arruda, H. M. Yang, A model for interactions between immune cells and HIV considering drug treatments, *Comp. Apl.Math.*, 37, 282-295, 2018. <https://doi.org/10.1007/s40314-017-0528-8>
- [26] G. L. Patrick, *An introduction to medicinal chemistry*, Oxford University Press, Oxford, 2013.
- [27] E. Polak, *Optimisation. Algorithms and consistent approximations*, AMS, V.124, Springer.
- [28] Rong L, Gilchrist MA, Feng Z, Perelson AS, Modeling within host HIV-1 dynamics and the evolution of drug resistance: Trade-offs between viral enzyme function and drug susceptibility, *J. Theor. Biol.* 247:804–818, 2007.
- [29] Shu H, Wang L, Watmough J, Sustained and transient oscillations and chaos induced by delayed antiviral immune response in an immunosuppressive infection model, *J. Math. Biol.* 68:477–503, 2014.
- [30] M A Stafford, L Corey, Y Cao, E S Daar, D D Ho, A S Perelson, Modeling plasma virus concentration during primary HIV infection, *J Theor Biol.* 2000 Apr 7;203(3):285-301. doi: 10.1006/jtbi.2000.1076.
- [31] Nowak MA, Bonhoeffer S, Shaw GM, May RM, Anti-viral drug treatment: dynamics of resistance in free virus and infected cell populations, *J. Theor. Biol.* 184:203-217, 1997.
- [32] Kepler TB, Perelson AS, Drug concentration heterogeneity facilitates the evolution of drug resistance, *Proc. Natl. Acad. Sci. USA* 95:11514–11519, 1998.
- [33] Smith RJ, Wahl LM, Distinct effects of protease and reverse transcriptase inhibition in an immunological model of HIV-1 infection with impulsive drug effects, *Bull. Math. Biol.* 66:1259–1283, 2004.
- [34] Ouifki R, Witten G, A model of HIV-1 infection with HAART therapy and intracellular delay, *Discrete Cont. Dyn-B* 8:229–240, 2007.
- [35] A. N. Tikhonov, On the stability of inverse problems (in Russian), Doklady of the USSR Academy of Science 39 (1943), 195–198.

- [36] A. N. Tikhonov and V. Ya. Arsenin, *Solutions of Ill-Posed Problems*, Winston and Sons, Washington, DC, 1977.
- [37] A. N. Tikhonov, A. V. Goncharsky, V. V. Stepanov and A. G. Yagola, *Numerical Methods for the Solution of Ill-Posed Problems*, London: Kluwer, London, 1995.
- [38] UNAIDS, <http://aidsinfo.unaids.org>
- [39] A. W. C. Yan, P. Cao, J. M. McCaw, On the extinction probability in models of within-host infection: the role of latency and immunity, *J Math Biol.*, 73:787-813, 2016.
- [40] Matlab source code AFEM_HIV, https://github.com/ProjectWaves24/AFEM_HIV_3eq